State of stress in areas of active unconventional oil and gas development in North America

Jens-Erik Lund Snee and Mark D. Zoback

ABSTRACT

In this paper, we present comprehensive data on stress orientation and relative magnitude in areas throughout North America where unconventional oil and gas are currently being developed. We find excellent agreement between maximum horizontal principal stress (S_{Hmax}) orientations over a wide range of depths, using multiple methods. In all basins studied, we observed coherent stress fields that in some cases vary systematically from one part of a basin to another. In the Appalachian Basin in the eastern United States, S_{Hmax} is oriented northeast–southwest to east-northeast–west-southwest and the style of faulting is compressive, transitioning from reverse faulting in eastern Pennsylvania and New York to principally strike-slip faulting in western Pennsylvania, Ohio, and West Virginia. In the midcontinent, central Oklahoma is characterized by an approximately east–west S_{Hmax} direction and strike-slip faulting. The Fort Worth Basin in northeastern Texas is characterized by normal–strike-slip faulting and a north-northeast–south-southwest S_{Hmax} direction. In the Midland subbasin of western Texas, S_{Hmax} is consistently approximately east–west and normal–strike-slip faulting is observed. Farther west, the Delaware subbasin of western Texas and southeastern New Mexico is characterized by normal faulting and S_{Hmax} rotates ~150° clockwise from north to south. Marked changes in S_{Hmax} direction also occur across the Raton Basin of southern Colorado and northern New Mexico, the Denver-Julesburg Basin in northern Colorado, and the Uinta Basin in northeastern Utah, likely associated with their location near the margins of extensional provinces. The new data sets we present help improve operational efficiency by constraining absolute stress magnitudes and the ideal azimuth to drill horizontal wells (i.e., perpendicular to the local S_{Hmax} orientation) and make it possible to predict which fractures and faults are likely to be activated during hydraulic stimulation.

Manuscript received September 7, 2020; provisional acceptance February 12, 2021; revised received April 4, 2021; final acceptance April 23, 2021.
DOI:10.1306/08102120151

AUTHORS

JENS-ERIK LUND SNEE ~ *Department of Geophysics, Stanford University, Stanford, California; present address: Geosciences and Environmental Change Science Center, US Geological Survey, Denver, Colorado; jlundsnee@usgs.gov*

Jens-Erik Lund Snee is a Mendenhall Research Fellow at the US Geological Survey studying the stress field, induced seismicity, and tectonic history. He holds a Ph.D. in geophysics and an M.S. degree in geological and environmental sciences from Stanford University. His experience includes work for Statoil (Equinor) and the US Forest Service, and a Fulbright Fellowship to New Zealand.

MARK D. ZOBACK ~ *Department of Geophysics, Stanford University, Stanford, California; zoback@stanford.edu*

Mark D. Zoback is the Benjamin M. Page Professor of Geophysics at Stanford University. Mark is the author of two textbooks and the author or co-author of approximately 400 technical papers. Mark conducts research on in situ stress, fault mechanics, and reservoir geomechanics with an emphasis on unconventional oil and gas production, induced seismicity, and CO_2 sequestration.

ACKNOWLEDGMENTS

The data set presented here is based on generous contributions of maximum horizontal principal stress orientation data previously provided to us by several individuals and oil, gas, and geothermal energy companies including AltaRock Energy, Apache Corporation, ConocoPhillips, Cyrq Energy, MicroSeismic, Inc., Ovintiv, Inc. (Newfield Exploration Company), Robert Cornell, Ryan Thompson, and Whiting Petroleum Corporation. Helpful discussions with Ankush Singh and Wenhuan Kuang improved the manuscript. We thank AAPG Editor Robert K. Merrill for editorial work and Tricia Allwardt, Debra Higley, and three anonymous reviewers for excellent comments. Funding was provided by the Stanford Center for Induced and Triggered Seismicity. Any use of trade, firm, or product

names is for descriptive purposes only and does not imply endorsement by the US Government.

DATASHARE 143

Tables S1–S3 are available in an electronic version on the AAPG website (www.aapg.org/datashare) as Datashare 143.

INTRODUCTION

Knowledge of the Earth's stress field is an important factor affecting production of oil, gas, and geothermal resources. This is true for conventional development, but it is especially true for unconventional development involving multistage hydraulic fracturing in horizontal wells. The stress field controls the orientation of hydraulic fractures as well as the pressure needed to initiate and propagate the hydraulic fractures away from the wellbores. Understanding the initial stress anisotropy (i.e., the differences in magnitude between the vertical stress [S_V], maximum horizontal principal stress [S_{Hmax}], and minimum horizontal stress [S_{hmin}]) allows us to predict the degree to which poroelastic stress changes that are induced by reservoir depletion could affect the success of subsequent stimulation. Finally, understanding the stress field allows one to predict how preexisting fractures slip during hydraulic fracturing stimulation and to identify the potential importance of larger faults that might be activated by produced water injection or hydraulic fracturing.

Here we present detailed maps of the stress field in the parts of North America that are of primary interest for unconventional oil and gas development. The maps include hundreds of new measured orientations of S_{Hmax} and the first comprehensive and quantitative representation of the faulting regime (relative principal stress magnitudes) across North America (Figure 1). As we show, knowledge of relative stress magnitude (A_ϕ) values and pore pressure (P_P), together with reasonable assumptions about crustal strength, can provide the bounding limits on absolute stress magnitudes. In the first part of this paper, we present the state of stress in intraplate North America and explain how to interpret the maps, including how to employ the mapped A_ϕ values to determine limits on absolute stress magnitudes at any location. In the second part of the paper, we provide detailed and greatly enhanced information about the state of stress in eight operational areas.

Figure 1 presents an updated overview of the state of stress across central North America (after Lund Snee and Zoback, 2020a). The black lines represent measured orientations of S_{Hmax} that were obtained using a variety of types of indicators described in Appendix 1. The azimuths of the lines represent the orientations of S_{Hmax} at each specific location. The length of each line is based on a rigorous quality ranking procedure also discussed in Appendix 1. It is important to recognize that each wellbore stress measurement on the map represents numerous consistent observations that, for wellbore measurements, span a significant range of depths. Two techniques that have only recently become viable for widespread use are (1) orientations of legacy hydraulic fractures (from subvertical wells) as observed in modern horizontal wells and (2) orientations of clouds of microseismic events that delineate

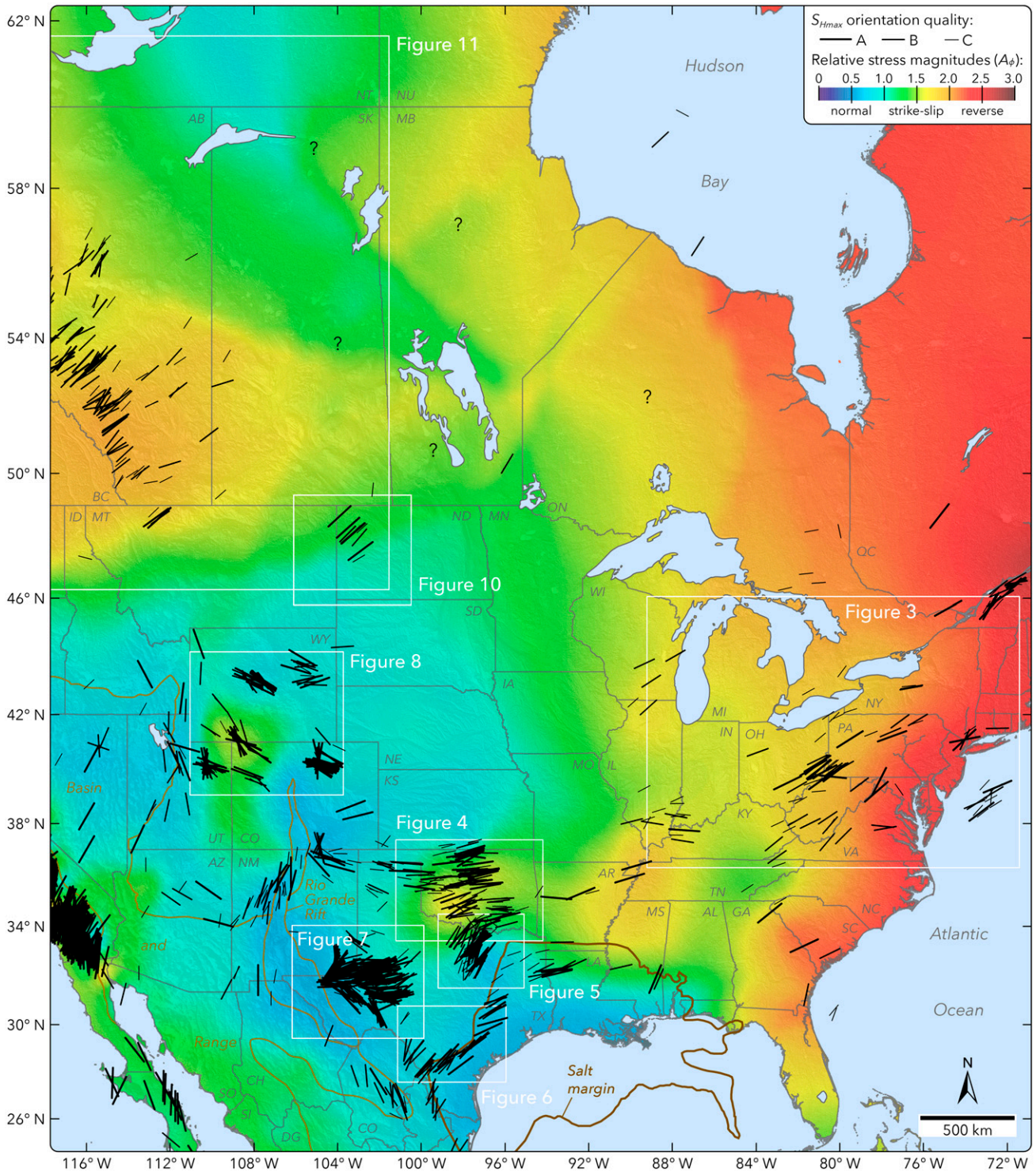

Figure 1. State of stress in central and eastern North America, showing orientations of the maximum horizontal principal stress (S_{Hmax}) and the style of faulting (A_ϕ). Data are principally from the World Stress Map (Heidbach et al., 2018), Lund Snee and Zoback (2020a), and sources therein, but also include several new S_{Hmax} orientations. The Gulf of Mexico salt margin is after Pindell and Kennan (2009).

propagating hydraulic fractures during reservoir stimulation. As we discuss in detail when we present individual regions, the stress measurements are quite consistent between the various types of indicators and at various depths. The colored background in Figure 1 (and subsequent maps) depicts the relative magnitudes of the three principal stresses. As discussed by Lund Snee and Zoback (2020a), focal mechanism stress inversions were used to determine stress orientations only when a group of reliable earthquake focal plane mechanisms was available in a localized area. However, A_ϕ values were determined using both focal mechanism inversions and individual (or small groups of) focal plane mechanisms, both natural and potentially induced, as well as indicators of currently active faulting.

Most data presented in this paper are from a greatly expanded data set presented by Lund Snee and Zoback (2020a). That study included approximately 300 new S_{Hmax} orientations and presented the first-ever map of both stress orientation and A_ϕ values across the North American continent. Here we also provide 11 previously unpublished S_{Hmax} orientations and newly include 4 S_{Hmax} orientations from Schwab et al. (2017). Figure 1 shows those new data (Tables S1, S2, supplementary material available as AAPG Datashare 143 at www.aapg.org/datashare) together with the previously available S_{Hmax} orientations including from the World Stress Map (Heidbach et al., 2018). In this paper, we describe the state of stress specifically within the basins in North America that are currently areas of significant unconventional oil and gas development.

USE OF THE A_Φ PARAMETER TO QUANTITATIVELY DESCRIBE THE STYLE OF FAULTING

The state of stress at any location can be simply described by the orientations and magnitudes of three mutually perpendicular principal stresses. It is convenient to represent the stress field in terms of the three principal stresses, which are generally horizontal and vertical in the Earth's brittle upper crust (Anderson, 1951). Several studies have confirmed this assumption (Zoback and Zoback, 1980, 1989; Zoback, 1992, 2007; Peška and Zoback, 1995; Heidbach et al., 2018; Lund Snee and Zoback, 2018, 2020a; Lund Snee, 2020).

As originally shown by Anderson (1951), the style of faulting active in an area is determined by the relative magnitudes of the principal stresses. Normal (extensional) faulting occurs when $S_V > S_{Hmax} > S_{hmin}$, strike-slip faulting (SS) occurs when $S_{Hmax} > S_V > S_{hmin}$, and reverse (compressional) faulting occurs when $S_{Hmax} > S_{hmin} > S_V$. Because the relative magnitude of three values cannot be expressed using a simple ratio, Simpson (1997) developed the following parameter to express their relationship:

$$A_\phi = (n + 0.5) + (-1)^n(\phi - 0.5) \quad (1)$$

where

$$\phi = \frac{S_2 - S_3}{S_1 - S_3} \quad (2)$$

and where S_1, S_2, and S_3 are the maximum, intermediate, and minimum principal stresses, respectively, with $n = 0$ for normal faulting (NF), $n = 1$ for SS, and $n = 2$ for reverse faulting (RF). The ϕ parameter, which ranges between 0 and 1, was originally defined by Angelier (1979) to indicate the relative magnitude of S_2 with respect to S_1 and S_3. Its value controls the direction of slip on a given fault.

Where sufficient numbers of well-constrained focal mechanisms are available in an area (typically more than 20–25), they can be formally inverted to find the orientation of the three principal stresses (and thereby the n value) and the ϕ parameter that are most consistent with the orientation of the faults that slipped and their observed slip directions. Although several authors have proposed different methodologies for inverting focal plane mechanisms for stress, we use here the joint inversion technique of Vavryčuk (2014) because it applies an iterative approach to discriminate which nodal plane represents the active fault plane and which is the auxiliary nodal plane. We determined the uncertainties of the calculated stress orientations and ϕ values using bootstrap sampling of the input earthquake focal mechanisms. Bootstrap sampling involves randomly sampling the inputs, in this case individual focal mechanisms used for the inversion, with replacement, meaning that any input mechanism could be sampled once, more than once, or not at all. The

result is computed, and this process is repeated a specified number of times B, in this case with B = 1000, to yield a distribution of outputs that can be used to estimate uncertainties.

Although stress inversions are good indicators of S_{Hmax} orientation and ϕ, their applicability is limited by the relative sparsity in most intraplate areas of earthquakes of sufficient number and the quality of their focal mechanisms. However, because focal plane mechanisms represent the style of faulting that produced each earthquake, even reliable focal plane mechanisms of relatively small earthquakes can provide valuable information for constraining A_ϕ within useful bounds. The principles for constraining A_ϕ were presented by Lund Snee and Zoback (2020a). As an example, if a single NF focal mechanism is available in an area, the faulting regime can be loosely constrained between radial NF (A_ϕ = 0) and NF–SS ($A_\phi \approx 1.25$). These bounds provide the full permissible uncertainty ranges. A best estimate (e.g., the mean value of an uncertainty distribution, to be plotted on maps) from within this range can be based on any additional information (e.g., recognizing that radial NF is extremely rare or employing geologic observations of active NF in the area). If additional mechanisms become available nearby, the constraints can be tightened, and the best estimate can be refined. For instance, if a second event occurred yielding a purely strike-slip mechanism in addition to the first NF mechanism, then it would be clear that the faulting regime is broadly NF–SS (approximately $0.75 \le A_\phi \le 1.25$). Additional focal mechanisms might indicate that NF events occurred more commonly, for example, allowing for improved estimates of the most likely A_ϕ value and narrower uncertainty bounds. Lund Snee and Zoback (2020a) assumed mostly Gaussian uncertainty ranges for A_ϕ, truncated by the maximum and minimum permissible bounds. The supplement to that paper shows A_ϕ uncertainties and the distribution of A_ϕ control points in graphical form.

The colored backgrounds in the stress maps presented in this paper were created by interpolating between individual data points that were estimated using this approach. The focal mechanism catalog employed for that study (Table S3, supplemental material available as AAPG Datashare 143 at www.aapg.org/datashare, with a few additional mechanisms for western Texas) was compiled from several sources across North America (Dziewoński et al., 1981; Kao et al., 1998, 2012; Kao and Jian, 1999; Braunmiller and Nábělek, 2002; Ichinose et al., 2003; Ristau et al., 2003, 2007; Mazzotti and Townend, 2010; Herrmann et al., 2011; Ekström et al., 2012; Hauksson et al., 2012; Yang et al., 2012; Eaton and Mahani, 2015; Singh et al., 2015; Scales et al., 2017; US Geological Survey Earthquake Hazards Program, 2017; Quinones et al., 2018; Savvaidis et al., 2019), which were filtered according to procedures outlined by Lund Snee and Zoback (2020a). Other sources of data that were employed less commonly include Quaternary surface offsets on faults (Madole, 1988; Crone and Luza, 1990; Crone and Wheeler, 2000), evidence of pervasive active deformation (e.g., Ricketts et al., 2014), and microseismic focal mechanisms or stress inversions dominantly related to hydraulic fracturing operations that were provided by industry and compiled from individual studies. Stress magnitudes determined from wellbores were not employed for the A_ϕ maps because of the potential for viscous stress relaxation in certain lithologies to locally perturb A_ϕ values (see the discussion on this phenomenon below). The supplementary data tables (available as AAPG Datashare 143 at www.aapg.org/datashare) indicate whether the A_ϕ control points used to interpolate the style of faulting were based on individual mechanisms or small groups, formal stress inversions from larger groups, or other indicators of active faulting.

Lund Snee and Zoback (2020a) discuss the state of stress throughout the North American continent from the perspective of plate driving forces as well as forces arising from variations of lithospheric density, thickness, and thermal structure. The compressive stress field in eastern North America (SS and RF) is likely related to the relatively low geoid anomaly in this region, which is in part attributable to the effects of ongoing postglacial rebound (e.g., Mitrovica and Peltier, 1989). The generally extensional stress field in the western United States (NF and SS) is in large part attributable to high gravitational potential energy associated with thermally elevated crust and thinned lithosphere. The marked variations of S_{Hmax} orientation that occur over short distances (tens of kilometers) in the western United States, especially outside the margins of the Rio Grande rift (RGR) and Basin and Range (BRP) extensional provinces (Figure 1), indicate relatively shallow sources of stress, most likely density variations within the upper crust.

USE OF A_Φ TO DETERMINE THE LIMITS ON STRESS MAGNITUDES

Although the limiting magnitudes of S_{Hmax} or S_{hmin} are both of interest, in practice it is the value of S_{hmin} that is either known, or can be obtained, from some form of hydraulic fracturing, ideally mini-fracs or diagnostic fracture injection tests. It is especially challenging to directly estimate S_{Hmax} (see Zoback, 2007). Fortunately, the finite strength of the Earth's crust provides important constraints on principal stress magnitudes. The maximum permissible difference between principal stresses is determined by the strength of the faults that are best oriented for failure within the stress field, in accordance with Mohr-Coulomb failure theory (Jaeger et al., 2007). The coefficient of sliding friction (μ) on faults in most intraplate areas ranges from 0.6 to 1.0 for most rock types and is commonly nearly 0.6 (Byerlee, 1978). This Mohr-Coulomb frictional limit provides the bounds of S_{Hmax} and S_{hmin} that are possible for a given magnitude of S_V, and it can be described by the following equation (Jaeger et al., 2007) for a given P_P:

$$\frac{\sigma_1}{\sigma_3} = \frac{S_1 - P_P}{S_3 - P_P} = \left[(\mu^2 + 1)^{\frac{1}{2}} + \mu\right]^2 \approx 3.12 \qquad (3)$$

where σ_{ii} is simple "Terzaghi" effective stress ($\sigma_{ii} \equiv S_{ii} - P_P$) and S_{ii} are the diagonal (principal) components of the stress tensor.

By combining equations 1, 2, and 3, Appendix 2 provides the equations that allow the range of horizontal principal stress magnitudes to be expressed as a function of A_ϕ for known values of S_V and P_P.

Using known values of A_ϕ, one can estimate the permissible bounds on the absolute magnitudes of the principal stresses. Figure 2 shows how the limiting magnitudes of S_{Hmax} and S_{hmin} vary as a function of A_ϕ for two assumed values of P_P, hydrostatic pore pressure in the upper panel, and overpressure (P_P = 0.85 S_V) in the lower panel. Additional information is required beyond simply A_ϕ to determine the magnitudes of S_{Hmax} and S_{hmin}. To simplify and generalize this analysis with respect to depth, the limiting magnitudes of the values associated with S_{Hmax} and S_{hmin} are normalized by S_V, which is easy to measure because it requires only access to commonly available density logs. In Figure 2, note that the maximum horizontal stress anisotropy depends strongly on P_P as well as A_ϕ, as stress magnitudes are much more anisotropic at hydrostatic pore pressure. The way to interpret the results shown in Figure 2 is as follows:

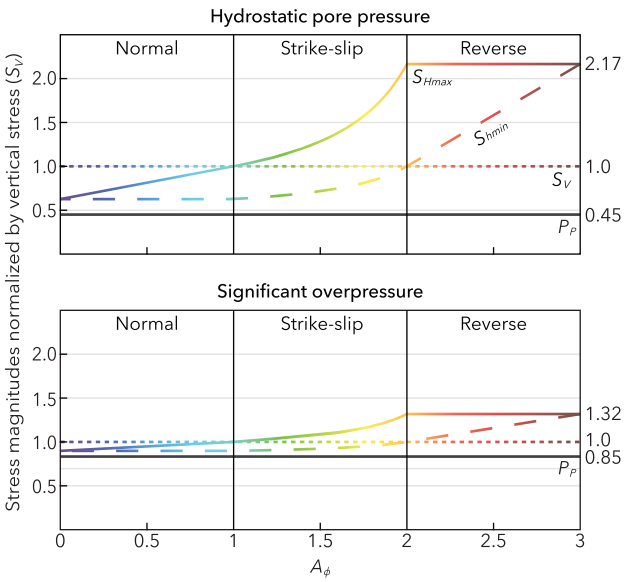

Figure 2. Relationship between relative stress magnitudes (A_ϕ) and the magnitudes of the three principal stresses (the vertical stress [S_V]; maximum horizontal stress [S_{Hmax}]; minimum horizonal stress [S_{hmin}]). The crust is assumed to be in a state of frictional failure equilibrium (which modulates differential stress magnitudes), with a coefficient of friction of 0.6. Stress magnitudes are normalized to S_V. The upper panel shows stress magnitudes for approximately hydrostatic pore pressures ($P_P = 0.45S_V$, equivalent to ~0.43 psi/ft if S_V is ~1.08 psi/ft). The lower panel shows stress magnitudes for strongly overpressured conditions ($P_P = 0.85S_V$, equivalent to ~0.92 psi/ft).

- In a NF regime ($S_V \geq S_{Hmax} \geq S_{hmin}$ and $1 \geq A_\phi \geq 0$), both S_V and S_{hmin} are constant and the value for S_{hmin} is a lower bound determined from equation 3 for the assumed value of P_P in each figure. The magnitude of S_{Hmax} varies linearly with A_ϕ.
- In a SS regime ($S_{Hmax} \geq S_V \geq S_{hmin}$ and $2 \geq A_\phi \geq 1$), S_V is constant and the values for S_{hmin} and S_{Hmax} are determined from equation 3 and equation 17 in Appendix 2, respectively, for the assumed value of P_P in each figure.
- In a RF regime ($S_{Hmax} \geq S_{hmin} \geq S_V$ and $3 \geq A_\phi \geq 2$), S_V and S_{Hmax} are constant and the value for S_{Hmax} is an upper bound as determined from equation 3 for the assumed value of P_P in each figure. The magnitude of S_{hmin} varies linearly with A_ϕ.

Several lines of evidence indicate that the principal stresses are at the frictional limit (rather than simply constrained by it) in brittle rocks of the upper crust; included are brittle sedimentary, crystalline, and metamorphic rocks, either at relatively shallow depth or in the underlying basement. In other words, brittle rocks in the crust are in a state of frictional failure equilibrium, in which the subsets of natural faults that are optimally oriented for frictional sliding in the current stress field are critically stressed and commonly within one earthquake cycle of failure (Zoback et al., 2002). Although frictional failure equilibrium applies generally to the strong rocks that form most of the Earth's brittle upper crust, more ductile lithologies, including clay- and carbonate-rich reservoir rocks, are known to experience stress relaxation over geologic time because of viscous creep (Friedman and Heard, 1974; Warpinski, 1983; Swolfs, 1984; Sone and Zoback, 2013, 2014; Rassouli and Zoback, 2018). As a consequence, the differential stresses measured within these specific lithologies can be considerably lower than those of stiffer bounding rocks (Sone and Zoback, 2014; Zoback and Kohli, 2019) because the horizontal stress magnitudes converge over time toward S_V (which is equal to the overburden and therefore cannot change). It is not currently known whether the magnitude of S_{Hmax} approaches S_V at a rate proportional to S_{hmin}. However, A_ϕ may vary between brittle and ductile lithologies (see e.g., Ma and Zoback, 2020), suggesting that creep may locally affect A_ϕ in clay-rich strata. The effects of viscous stress relaxation pose considerable implications for development of unconventional oil and gas resources, which are commonly produced from clay- and carbonate-rich rocks, because they imply high fracture gradients and difficulty initiating hydraulic fractures and maintaining open fracture networks in clay formations (e.g., Singh et al., 2019; Xu et al., 2019; Zoback and Kohli, 2019). However, despite the implications for stress magnitudes, the orientation of S_{Hmax} is generally unaffected by differences in lithology (as first shown by Zoback and Zoback, 1980).

STATE OF STRESS IN INTRAPLATE NORTH AMERICA

Figure 1 shows that the state of stress is broadly compressive throughout eastern North America. Along the eastern seaboard, RF is dominant and S_{Hmax} is oriented approximately northeast–southwest. Moving west, the faulting regime becomes increasingly less compressive, transitioning to SS–RF on the west side of Hudson Bay in Canada and inland parts of the eastern United States, and then to dominantly SS in parts of Oklahoma, the midwestern United States, and central Canada. Moving west over this part of the central and eastern United States, S_{Hmax} rotates gradually and systematically clockwise to become nearly east–west in the central and southern Great Plains.

The western United States is mostly extensional, with NF and SS active over most of the region. In these extensional areas, S_{Hmax} rotates over much shorter distances, in a few cases nearly 90° over tens of kilometers near the margins of the RGR and BRP extensional domains (Lund Snee and Zoback, 2018, 2020a). Although data are sparse in southern Canada, the faulting regime is generally compressive, with RF–SS and SS active in British Columbia and Alberta (see also Fox and Soltanzadeh, 2015; Shen et al., 2019; Zhang et al., 2019). The orientation of S_{Hmax} is approximately northeast–southwest across a broad region that covers Alberta, northern Montana, and the northern Great Plains, and which may extend eastward into Ontario (Reiter et al., 2014; Heidbach et al., 2018; Lund Snee and Zoback, 2020a). In the sections below, we describe how the mapped variations in the stress field affect each of the

major areas of unconventional oil and gas development in North America.

In addition to their potential for unconventional oil and gas development, many areas in the western United States are also prospective for conventional and enhanced geothermal energy. These areas include (but are not limited to) the eastern and western margins of the BRP and the Imperial Valley of southernmost California, where crustal heat flow is strongly elevated (Blackwell et al., 2011). As shown in Figure 1, S_{Hmax} is oriented approximately north-northeast–south-southwest throughout much of the United States part of the BRP. The faulting regime becomes more compressive westward, from NF with an appreciable SS component across much of the domain to NF–SS with SS dominant in western and southern Nevada and eastern California. Within the Imperial Valley, the faulting regime is generally SS and S_{Hmax} varies between approximately north–south to northeast–southwest, although there is considerable spatial variability (Yang and Hauksson, 2013; Lund Snee and Zoback, 2020a). The presence in the Imperial Valley and other parts of California of major plate-bounding fault zones, which may be frictionally weak (μ potentially much less than 0.6) and hence subject to different mechanical behavior than intraplate faults (Lachenbruch and Sass, 1980; Zoback et al., 1987; Mount and Suppe, 1992; Lockner et al., 2011) locally affects the state of stress in this area (e.g., Townend and Zoback, 2004).

STATE OF STRESS IN AREAS OF UNCONVENTIONAL DEVELOPMENT

The Central and Eastern United States

Figure 3 shows the stress field across the central and eastern United States and southeastern Canada. This region includes the Appalachian Basin, which

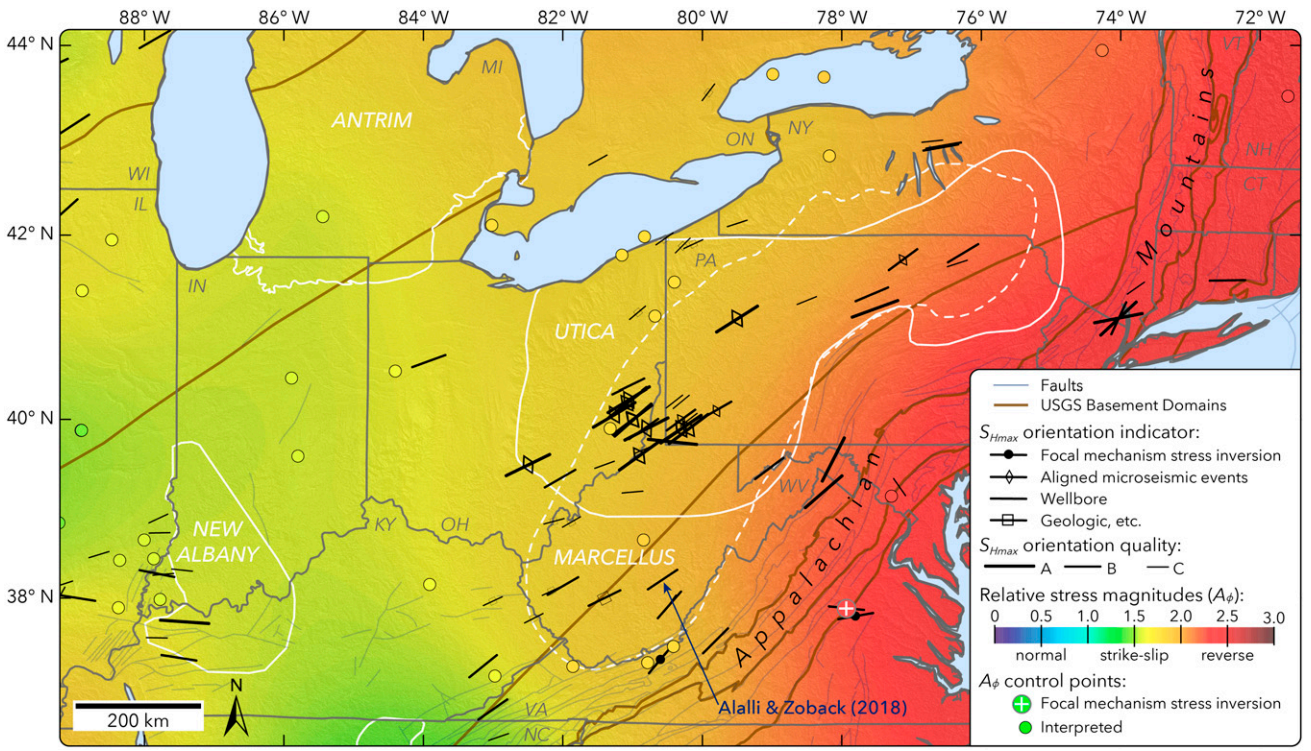

Figure 3. State of stress in the eastern United States and southeastern Canada. Control points for relative stress magnitudes are colored by the value of A_ϕ interpreted for each. The maximum horizontal principal stress (S_{Hmax}) orientation in southeastern West Virginia indicated with a reference to Alalli and Zoback (2018) is approximately where that study suggested that both horizontal and vertical hydraulic fractures developed during reservoir stimulation at a single well pad. US Geological Survey (USGS) basement domain boundaries are from Lund et al. (2015). Faults are from the Geologic Map of North America (Reed et al., 2005; Garrity and Soller, 2009). Play outlines are from the US Energy Information Administration. See Figure 1 for map location and additional references.

is the most prolific source of shale gas in the United States although it produces very little oil (US Energy Information Administration, 2020). Most production is from the Middle Devonian Marcellus Shale, an interval composed dominantly of thick marine mudstones with interbedded limestone (Zagorski et al., 2012). Gas is also produced from the Ordovician Utica and Point Pleasant Formations (e.g., Kirschbaum et al., 2012). The region also includes the Upper Devonian Antrim Shale of the northern Michigan Basin and the Devonian New Albany Shale of the Illinois Basin, both of which are sources of biogenic gas (e.g., Martini et al., 1998; Curtis, 2002).

As seen in Figure 3, S_{Hmax} is predominantly northeast–southwest to east-northeast–west-southwest, and it rotates gradually westward to approximately east-northeast–west-southwest and east–west in the midcontinent, including southern Indiana and western Kentucky (Figure 3). The general consistency of S_{Hmax} across major geologic structures in eastern North America was noted by Sbar and Sykes (1973), Haimson (1977), Zoback and Zoback (1980, 1989), and Evans (1989), and it is supported by the additional data contributed by Hurd and Zoback (2012) and Lund Snee and Zoback (2020a). However, whereas the dominant source of stress in this region appears to be plate-scale tectonic factors rather than local heterogeneities, S_{Hmax} varies gradually toward the Appalachians to be generally parallel to the orogenic belt, suggesting possible influence from the potentially more buoyant Appalachian crust (Zoback and Zoback, 1989; Lund Snee and Zoback, 2020a).

The state of stress along the eastern seaboard of the United States and southeastern Canada is considerably more compressive than most other areas of unconventional energy development discussed in this paper. As shown in Figure 3, RF and SS–RF are active along the eastern coast, including the eastern and northeastern parts of the Marcellus and Utica plays in eastern New York, eastern Pennsylvania, and northeastern West Virginia. The recent earthquake in Sparta, North Carolina (on August 9, 2020 in the northwestern part of the state), with a moment magnitude (M_W) of 5.1 occurred because of oblique reverse slip on a shallowly north-northwest–striking fault plane, indicating approximately east-northeast–directed compression (Herrmann et al., 2011; Lund Snee and Zoback, 2020b; US Geological Survey, 2020). These kinematics appear compatible with the mapped stress field in this area (Figure 1), with S_{Hmax} oriented east-northeast–west-southwest or northeast–southwest and active SS and RF. The faulting regime becomes increasingly less compressive westward, transitioning to dominantly SS in, for example, Indiana, Kentucky, southern Michigan, and western Ohio, including the area of the New Albany and southern Antrim shale plays.

Evaporite deposits of the upper Silurian Salina Group are present above the Utica Formation and below the Marcellus Shale in southwestern New York, western Pennsylvania, eastern Ohio, and northeastern West Virginia (Wiltschko and Chapple, 1977; Ryder et al., 2008, 2012). Evans (1989) suggested that these ductile deposits may partially decouple the stresses in the overlying sedimentary rocks from those in the underlying rocks because their instantaneous shut-in pressure measurements indicated higher S_{hmin} magnitudes (more compressive) in strata immediately above the Salina salt. However, he found that the orientation of S_{Hmax} does not vary significantly between the sedimentary and crystalline rocks. Moreover, the permissible S_{Hmax} orientations implied by earthquake focal mechanisms (typically ≥5-km depth) are compatible with those measured in the sedimentary rocks deposited above the salt (Figure 3).

In Figure 3, as well as the stress maps of other regions included below, we symbolize S_{Hmax} orientations differently depending on whether they were obtained using aligned microseismic events associated with hydraulic fracturing operations, formal focal mechanism stress inversions, geologic indicators, or wellbore techniques such as borehole breakouts, drilling-induced tensile fractures, shear-wave velocity anisotropy, and hydraulic fractures measured from wellbores. It can be seen from Figure 3 (and in the other stress maps) that the various techniques provide orientations that agree closely, including measurements collected using the relatively new techniques described above (aligned microseismic events defining hydraulic fractures and legacy hydraulic fractures from older reservoir development observed in recent horizontal wells). This is shown especially well in Oklahoma (discussed below), where the dense coverage of S_{Hmax} orientations employs various symbol types.

Horizontal hydraulic fractures are expected in some parts of the highly compressive eastern area of Figure 3, where $A_\phi > 2.0$ ($S_{Hmax} > S_{hmin} > S_V$), but vertical hydraulic fractures are expected to occur in most of the area, where $A_\phi < 2.0$ ($S_{Hmax} > S_V > S_{hmin}$). At a well pad in southeastern West Virginia where $A_\phi \approx 2.0$ (Figure 3), Alalli and Zoback (2018) showed that microseismic events indicate horizontal hydraulic fractures at some levels and vertical hydraulic fractures at others. This site is in the transition zone between the stress domains in which horizontal and vertical fractures would be created (Figure 3). Horizontal hydraulic fractures appear to have developed exclusively when perforations were within the Marcellus Shale because of viscous stress relaxation in that clay- and organic-rich unit, but not in the stiffer Cherry Valley and Onondaga Limestones. The occurrence of horizontal hydraulic fractures and a stress regime in which RF is active might pose challenges for unconventional oil and gas production from horizontal wells in the eastern and northeastern parts of the Appalachian Basin region; these factors could require appreciable well spacing to reduce interference between wells, could limit the thickness of the formation that could be exploited by a horizontal well, and would involve high fluid pressures during stimulation in excess of S_V (the least principal stress) to propagate hydraulic fractures.

Oklahoma, Including the SCOOP, STACK, and Merge Plays

Figure 4 shows the state of stress in Oklahoma and surrounding areas, a region that includes several conventional and unconventional hydrocarbon plays. Among the most significant of these in recent years are the South-Central Oklahoma Oil Province

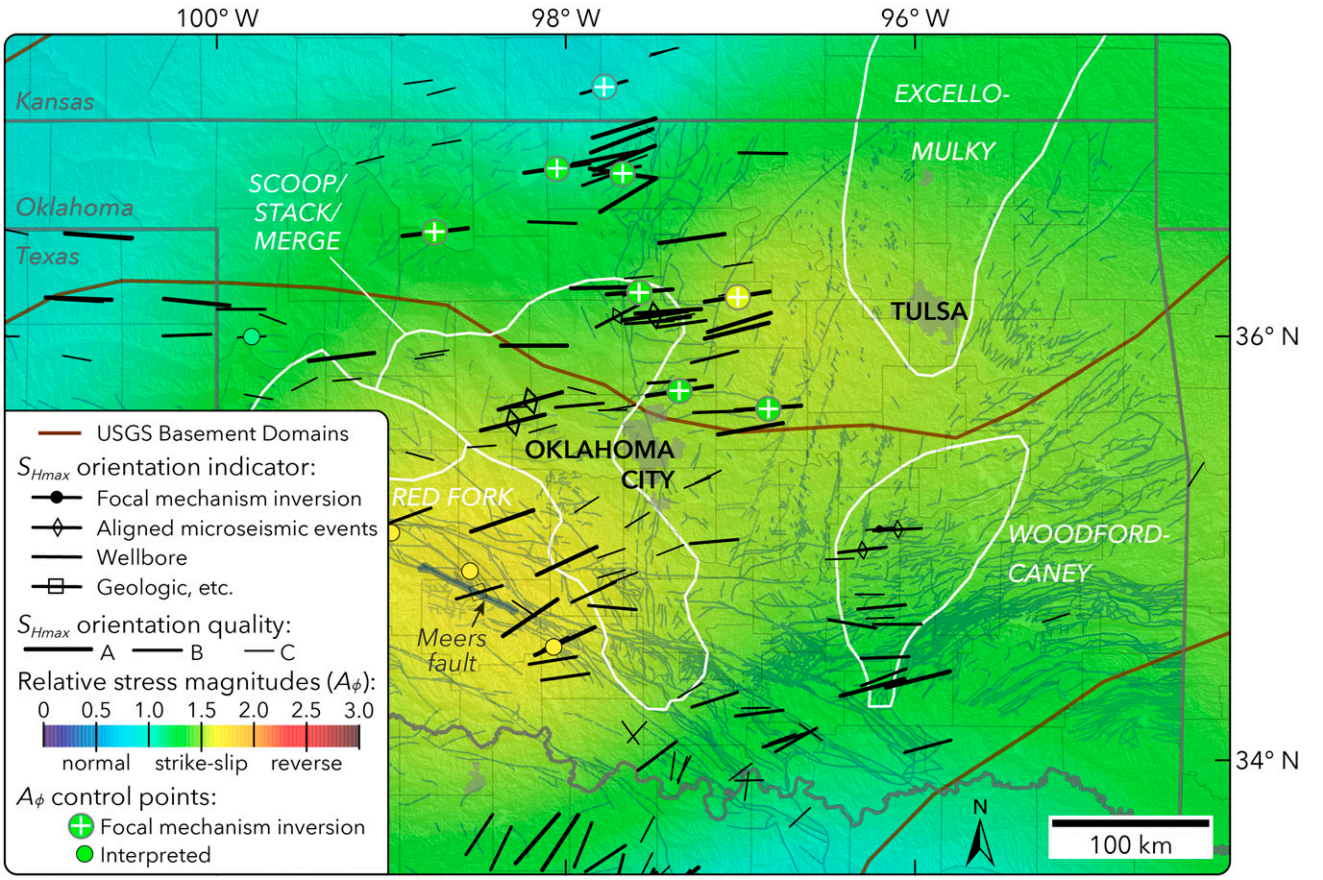

Figure 4. State of stress in Oklahoma and southern Kansas. The maximum horizontal principal stress (S_{Hmax}) orientations have been updated from the map published by Alt and Zoback (2017) to include additional data from Lund Snee and Zoback (2020a) and Schwab et al. (2017). Faults (fine lines) are from Ewing et al. (1990), Ewing and Lopez (1991), Crone and Wheeler (2000), and Darold and Holland (2015). See Figure 1 for map location. USGS = US Geological Survey.

(SCOOP), Sooner Trend Anadarko Basin, Canadian, and Kingfisher Counties (STACK), and "Merge" regions of the eastern Anadarko Basin, which collectively represent a significant source of both oil and gas (US Energy Information Administration, 2020). These regional plays comprise several shale and carbonate-bearing units, including the Middle Mississippian "Osage" and "Meramec" limestones and the predominantly Upper Devonian Woodford Shale source rocks (e.g., Harris, 1975). Thermal maturity of the Woodford Shale increases westward within the Anadarko Basin, with dry gas production occurring to the west and liquids to the east near Oklahoma City, with condensate in the intervening areas (Cardott, 2012).

The orientation of S_{Hmax} is consistently approximately east–west to east-northeast–west-southwest across most of central and northern Oklahoma but rotates ~70° counterclockwise southward from southcentral Oklahoma into northeastern Texas. In addition, S_{Hmax} rotates slightly counterclockwise southwestward from central Oklahoma to approximately east-northeast–west-southwest in the vicinity of the Meers fault, southwestern Oklahoma (Figure 4). Strike-slip faulting is dominant in central and eastern parts of Oklahoma, but the faulting regime becomes more extensional in northcentral Oklahoma, southcentral Kansas, and in the Texas panhandle. However, moving southwest from central Oklahoma, the faulting regime becomes more compressive, to SS–RF in southwestern Oklahoma, as indicated by oblique reverse slip on the Meers fault (Madole, 1988; Crone and Luza, 1990). The stress state in this part of southwestern Oklahoma appears to be considerably more compressive than nearby areas.

Beginning ca. 2009, seismicity increased sharply in central and northern Oklahoma and southcentral Kansas, predominantly because of disposal of very large volumes of saltwater coproduced with oil and gas into the deeper Arbuckle Group (Walsh and Zoback, 2015). More recently, Skoumal et al. (2018) showed that most of the seismicity specifically in the SCOOP, STACK, and Merge areas in central and western Oklahoma can be attributed to hydraulic fracturing operations. Thousands of earthquakes with magnitude levels ≥3 have occurred in Oklahoma in the past decade, including four with magnitude levels ≥5. The high density of focal mechanisms enabled Lund Snee and Zoback (2020a) to conduct stress inversions in eight areas within northern and central Oklahoma, yielding precise constraints on A_ϕ and S_{Hmax} orientation predominantly within the crystalline basement (colored dots with white crosses). As can be seen in Figure 4, there is good agreement between S_{Hmax} orientations from the focal mechanism inversions and those from the shallower sedimentary succession, which include borehole measurements (plain lines) and aligned microseismic events defining hydraulic fractures (lines with outward pointed triangles). The orientations of faults that have produced the widespread seismicity agree closely with fault orientations expected to be active based on the S_{Hmax} orientations that were measured in boreholes in the context of Coulomb faulting theory (Schoenball et al., 2018a, b).

The Fort Worth Basin, Northeastern Texas

Figure 5 shows the state of stress in the Fort Worth Basin (FWB), northeastern Texas. The FWB was one of the first areas where multistage horizontal drilling and hydraulic fracturing were economic for production of tight gas. Production has declined steadily since ca. 2012. The primary unconventional target in this region is the Mississippian Barnett Shale, which is a fine-grained, organic-rich marine deposit with widely varying mineralogy (e.g., Montgomery et al., 2005).

In general, S_{Hmax} is approximately northeast–southwest throughout the eastern and northern FWB. As noted above, S_{Hmax} rotates clockwise northward to be approximately east-northeast–west-southwest in southern Oklahoma (Figure 4). Despite the general consistency of S_{Hmax} orientations within the basin, there is a significant gradient in the faulting regime, from approximately SS in the north to NF–SS in much of the core area near and slightly north of Fort Worth, and finally NF–SS with a stronger component of NF ($A_\phi < 1.0$) from Fort Worth to the south.

The most productive part of the Barnett Shale play in the FWB is in Wise, Denton, and Tarrant Counties, which is approximately the area immediately north and northwest of Fort Worth (Figure 5) with the densest concentration of S_{Hmax} orientation measurements. This core area overlaps the strongest

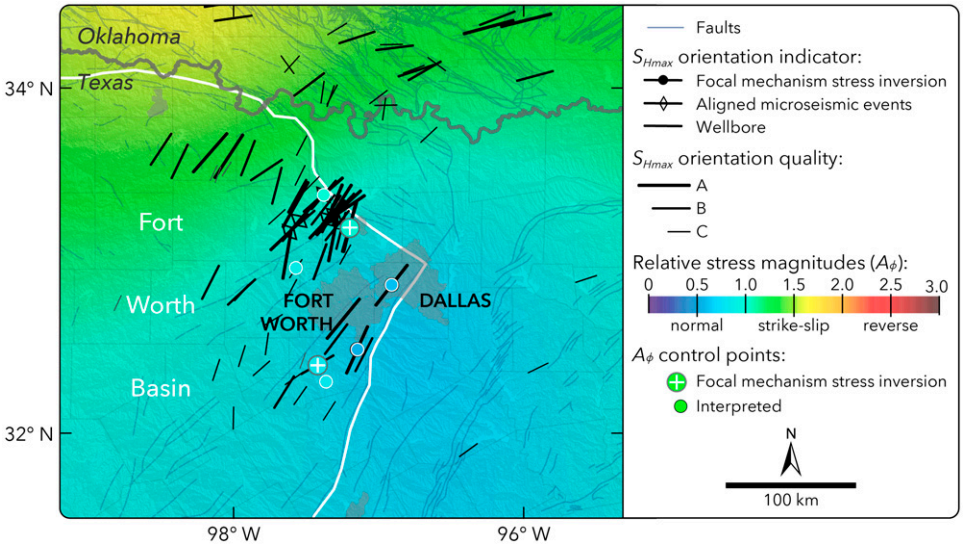

Figure 5. State of stress in the Fort Worth Basin, northeastern Texas. The data have been updated from those published by Lund Snee and Zoback (2016) to include more maximum horizontal principal stress (S_{Hmax}) orientations and an improved map of A_ϕ from Hennings et al. (2019) and Lund Snee and Zoback (2020a). Unlike the map by Lund Snee and Zoback (2016), the updated data set does not incorporate stress magnitudes measured in boreholes. Faults are from Ewing et al. (1990), Ewing and Lopez (1991), Crone and Wheeler (2000), and Darold and Holland (2015). See Figure 1 for map location.

petroleum system components, including elevated hydrogen index and thermal maturity (Montgomery et al., 2005; Jarvie et al., 2007; Zhao et al., 2007). However, these favorable qualities also extend considerably to the southwest of the core area, and Bowker (2003) noted that production varies across areas that have high gas saturation, suggesting that favorable production in the core area is influenced by additional factors. The most prolific production is in areas with purported barriers to vertical hydraulic fracture growth (Bowker, 2003, 2007; Pollastro et al., 2003; Montgomery et al., 2005). These potential barriers include the underlying Upper Ordovician Viola Limestone (Decker, 1933) and Simpson Group (Statler, 1965), the overlying Pennsylvanian Marble Falls Formation limestone (Freeman, 1964; Wiggins, 1986), and the Forestburg limestone (informally named), which separates the upper and lower members of the Barnett Shale. Outside of the core area to the southwest, the Barnett rests unconformably on karsted carbonates of the Ordovician Ellenburger Group.

Despite the spatial overlap between the core area and these purported fracture barriers, Fisher and Warpinski (2012) observed that many of the hydraulic fractures that propagate farthest out of zone below the northeast-dipping Barnett are where it is deepest (in the northeast part of the basin); in other words, fractures may propagate far out of zone within the core area despite the presence of these purported fracture barriers (Pollastro et al., 2007). Furthermore, laboratory study of samples from the northeastern FWB by Sone and Zoback (2014) found that the clay- and kerogen-bearing Barnett Shale in this region experiences viscous stress relaxation that could lead to an increase in the magnitude of S_{hmin} within that unit, requiring increased fluid pressures to develop and propagate hydraulic fractures. This could lead to appreciable out-of-zone fracture growth if these hydrofracs reached the stiffer overlying and underlying limestones, where the frac gradient might be considerably lower. In other words, these surrounding limestone units might serve here to promote rather than limit fracture growth and hence productivity. Consequently, the factors responsible for favorable production in the core area remain undetermined.

We suggest that the change in faulting regime in this area may have significant impact on production as the Barnett core area is coincident with the region where NF and SS are both active. In purely NF or SS stress states ($A_\phi \approx 0.5$ or 1.5, respectively), only one set of conjugate faults is likely to be active. In contrast, with NF–SS ($A_\phi \approx 1.0$), two conjugate sets (one set of steeply-dipping faults that strike parallel to S_{Hmax} and another set of subvertical faults subtending ~30°

from S_{Hmax}) would be favorably oriented, potentially increasing the number of preexisting fractures that could become active and thereby contribute to the permeable fracture network that develops during hydraulic reservoir stimulation (see Zoback and Lund Snee, 2018). Although variable by location, it appears that fractures at the full range of potentially active orientations for the approximately northeast–southwest S_{Hmax} orientation in the FWB (subvertical fractures striking approximately north-northeast–south-southwest and approximately east-northeast–west-southwest and steeply-dipping faults striking approximately northeast–southwest) are present within the Barnett Shale in some areas (Gale et al., 2007; Vermylen, 2011; Hennings et al., 2019).

The Eagle Ford Trend, Texas Gulf Coast

The Upper Cretaceous Eagle Ford Group is a carbonate-rich marine source rock that was deposited along the Gulf Coast, and it is a major source of both oil and gas (e.g., Mullen et al., 2010). The Eagle Ford can be divided into a more carbonate-rich and potentially stiffer upper member, and a more clay-rich and possibly less stiff lower member. The upper member is present only in the southwestern part of the United States play trend outlined in Figure 6, where the full Eagle Ford unit is significantly thicker (Tian et al., 2013). Stratigraphic units in this region dip toward the Gulf of Mexico, and thermal maturity within the Eagle Ford increases downdip to the southeast (US Energy Information Administration, 2014). Deposits along the inboard part of the trend contain oil, whereas dry gas is produced in the deeper strata, toward the Gulf of Mexico, with oil condensates in the intervening areas.

Figure 6 shows the state of stress along the western United States Gulf Coast, including the Eagle Ford trend. The orientation of S_{Hmax} is broadly parallel to the margin, and the sedimentary rocks on the Gulf coastal plain experience extension toward the Gulf of Mexico, predominantly accommodated by normal offset along growth faults. In general, NF (with a lesser strike-slip component) is dominant along the western Gulf Coast in the region of the Eagle Ford trend, but SS appears to become slightly more prevalent toward the southwest, based on regional trends (Figure 1) and limited local data.

It is important to note that most of the S_{Hmax} measurements in this area were obtained from within

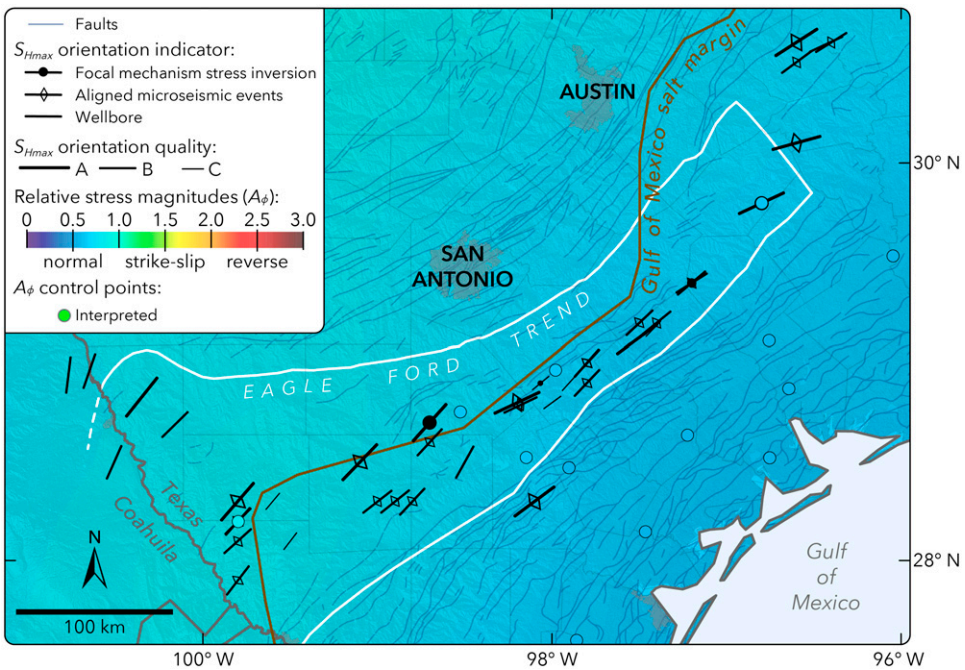

Figure 6. State of stress in the Eagle Ford trend, Texas Gulf Coast. The Gulf of Mexico salt margin is after Pindell and Kennan (2009). Faults are from Ewing et al. (1990) and Ewing and Lopez (1991). See Figure 1 for map location. S_{Hmax} = maximum horizontal principal stress.

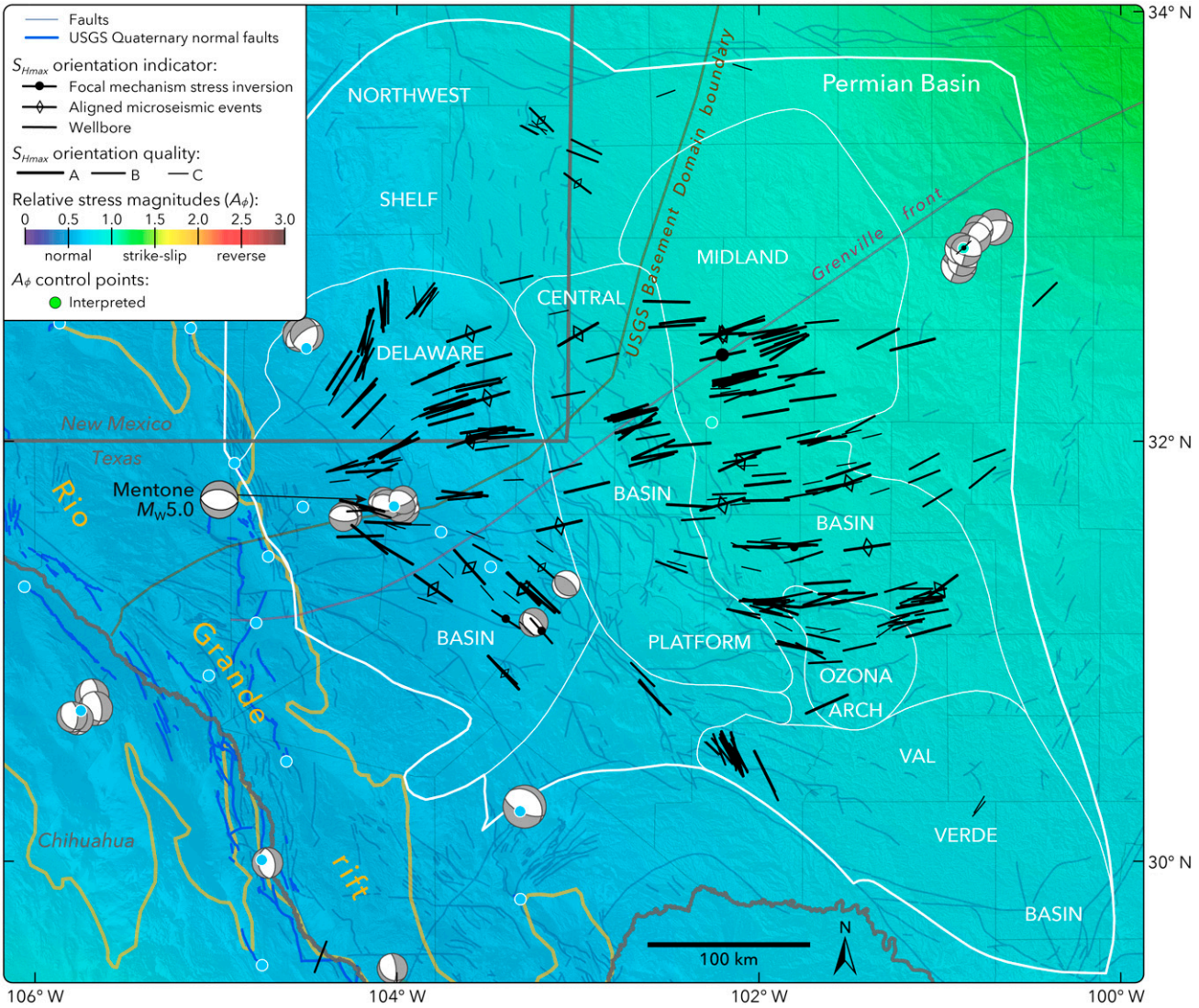

Figure 7. State of stress in the Permian Basin, western Texas and southeastern New Mexico. The map has been updated from the versions published by Lund Snee and Zoback (2016, 2018) to include more maximum horizontal principal stress (S_{Hmax}) orientations and an improved map of A_ϕ that excludes borehole measurements of stress magnitudes. The boundary between the Shawnee and Mazatzal basement domains is from Lund et al. (2015) and the Grenville front is from Thomas (2006). Light blue faults are from Ewing et al. (1990), Green and Jones (1997), and Ruppel et al. (2005). Bold, bright blue faults have experienced normal-sense offset during Quaternary time (Crone and Wheeler, 2000). Subdomain boundaries are from the Texas Bureau of Economic Geology Permian Basin Geological Synthesis Project. Focal mechanisms (principally from Herrmann et al., 2011) illustrate how the nodal plane orientations rotate southward across the basin consistent with the S_{Hmax} orientation indicators from the sedimentary succession. See Figure 1 for map location. M_W = moment magnitude; USGS = US Geological Survey.

the sedimentary succession above the ductile Louann Salt, which may decouple the stresses within the sedimentary succession from those in the underlying crystalline basement. Consequently, the area of the Gulf coastal plain that is southeast of the salt margin (Figure 6) is one of the few areas in which the stress measurements may not represent the state of stress in the crystalline rocks. Despite this, the focal mechanisms (e.g., Herrmann et al., 2011; Savvaidis et al., 2019) and recently obtained S_{Hmax} orientations mapped along or landward of the salt margin in Figure 6 agree closely with those obtained from above

the Louann Salt nearby, suggesting that there may be little difference in the state of stress between the shallower sedimentary and deeper crystalline rocks, at least in areas relatively near the salt margin.

The Permian Basin, Western Texas and Southeastern New Mexico

The Permian Basin of southeastern New Mexico and western Texas (Figure 7) is a structurally complex region and the largest actively producing source of tight oil in the United States (US Energy Information Administration, 2020). The basin can be divided into several subdomains, including the Northwest shelf and the Delaware and Midland subbasins, which have been the most active targets for unconventional development, and the Central Basin platform (CBP), where conventional oil and gas development has occurred but where there is currently little unconventional development.

The presently high rates of production in the Permian Basin can be largely attributed to the occurrence of several stacked, organic-rich shales, notably the informally named Upper Pennsylvanian–lower Permian Wolfcamp shale (e.g., King and King, 1929; Smith, 1929), the lower Permian Bone Spring Formation (e.g., Skinner, 1946; Montgomery, 1997), and the early Permian Spraberry Formation (e.g., Schmitt, 1954). These deposits are especially thick and productive within the clastic-dominated Delaware and Midland subbasins (basement-involved uplifts of the intervening CBP are capped primarily by shelf carbonates). Recent US Geological Survey assessments of undiscovered, technically recoverable unconventional reserves for the Bone Springs and Wolfcamp estimated 46 billion BOE, 8 trillion m^3 (280 trillion ft^3) of gas, and 20 billion bbl of natural gas liquids specifically within the Delaware subbasin (Gaswirth et al., 2018). Similar assessments for the Spraberry and Wolfcamp intervals in the Midland subbasin estimated technically recoverable totals of 24 billion BOE, 0.5 trillion m^3 (19 trillion ft^3) of gas, and 2 billion bbl of natural gas liquids (Gaswirth et al., 2016; Marra et al., 2017).

The state of stress in the Permian Basin is fairly consistent within the CBP and Midland subbasin. The faulting regime in these areas is generally NF–SS but becomes increasingly extensional to the west in the Delaware subbasin, where NF is prevalent. Lund Snee and Zoback (2016, 2018) showed that the Delaware subbasin has a remarkably complex stress field, but the high density of S_{Hmax} orientations reveal coherent and systematic changes from north to south. Unlike the central and eastern parts of the Permian Basin, orientations of S_{Hmax} rotate approximately 150° clockwise from the northern part of the basin going southward. Orientations of S_{Hmax} are approximately north–south in the north, approximately east–west in the middle of the Delaware subbasin, and approximately northwest–southeast in the southern part. As shown by the focal plane mechanisms (typically from earthquakes that occurred below the sedimentary succession), the complex stress field defined by the numerous wellbore stress indicators is characteristic of the stress field in the crystalline basement, as is generally observed elsewhere (e.g., Oklahoma in Figure 4).

Figure 7 shows the most reliable focal mechanisms available in the Delaware subbasin. Although dozens of mechanisms are currently available from the TexNet Seismic Monitoring Program (Savvaidis et al., 2019) in this basin, many of them appear strongly contradictory (e.g., NF and RF in the same area and NF mechanisms in the same area that display perpendicular nodal planes from one another) specifically in this area. Because no obvious criteria could be established for filtering them by quality, the mechanisms shown are principally from the Saint Louis University catalog (described by Herrmann et al., 2011). Figure 7 shows focal mechanisms for events that occurred through June 2020, including the March 26, 2020, M_W5.0 Mentone earthquake (see Lund Snee and Dvory, 2020; Savvaidis and Hennings, 2020). As can be seen in the figure, with one exception (a RF event near the boundary between the Delaware subbasin and CBP), NF focal mechanisms are observed in the central and southern Delaware subbasin, with nodal plane strikes rotating clockwise southward in close agreement with the mapped rotation of S_{Hmax} orientations over the same area.

The S_{Hmax} orientation in the eastern part of the Northwest shelf, at the border between New Mexico and Texas, is west-northwest–east-northeast, somewhat different from that to the south. Constraints on the extent of this stress domain are limited by the

sparse data in this area. The western part of the Val Verde subbasin (the southernmost part of the Permian Basin) has a stress state that is identical with that in the Delaware subbasin to the northwest but quite different from the approximately east–west S_{Hmax} orientation observed in the Ozona arch and southern Midland subbasin. Two orientations in the center of the Val Verde subbasin are approximately northeast–southwest, as seen in the Eagle Ford area farther to the southeast.

The state of stress in western parts of the Permian Basin, including the western Delaware subbasin and Northwest shelf, appears to be strongly influenced by the RGR immediately to the west (Figures 1, 7). The RGR is an area of approximately east–west rifting that is thought to have been active since the late Oligocene or early Miocene (Ingersoll, 2001; Ricketts et al., 2016). The profound rotation of S_{Hmax} within the Delaware subbasin and Northwest shelf could be an expression of a transition from dominantly approximately north–south S_{Hmax} orientations around the RGR to approximately east–west and east-northeast–west-southwest orientations that reflect the general state of stress in the central United States (Lund Snee and Zoback, 2020a).

The variability of the stress field in the Permian Basin is important for hydrocarbon development. For example, Rostami et al. (2020) showed that the orientation of Bakken Formation wells in the Williston Basin has a significant effect on well production, with the optimal orientation to drill horizontal wells being at the azimuth of S_{hmin}. As this direction varies dramatically from one area to another in the Delaware subbasin, it could significantly influence well production. Finally, as in the case of the FWB (see Hakso and Zoback, 2019), the large area of the Permian Basin that is characterized by relatively uniform S_{Hmax} orientations and both NF and SS, particularly the CBP and Midland subbasin, likely benefits from a greater proportion of fractures that are potentially active and hence permeable during stimulation (see Forand et al., 2017, for a compilation of fracture orientations across the Permian Basin).

The United States Intermountain West

The intermountain west hosts several sedimentary basins that contain significant tight oil and gas deposits, including the Green River, Uinta-Piceance, and Denver-Julesburg (DJ) Basins (see, e.g., US Geological Survey Uinta-Piceance Assessment Team, 2003; Higley et al., 2007; Johnson et al., 2011, 2016; Hawkins et al., 2016). The state of stress in this region is dominantly extensional (NF or NF–SS), although some areas are more compressive. Figure 8 shows that S_{Hmax} rotates markedly over short distances in parts of the western United States. In the central part of the region shown in Figure 8, from central Wyoming to central Colorado, S_{Hmax} typically ranges between west-northwest–east-southeast to west–east, albeit with some local variability. However, S_{Hmax} varies over relatively short distances in two areas, on the east and west sides of Figure 8, the DJ Basin in northeastern Colorado and the northern Uinta-Piceance Basin in northeastern Utah, and these variations are observed slightly outside the margins of extensional domains. The stress change observed within the Uinta-Piceance Basin occurs slightly to the east of the Basin and Range province (BRP) boundary (which is out of view to the west), within which S_{Hmax} is generally approximately north-northeast–south-southwest and the style of faulting is broadly NF–SS (but variable from NF to SS), as noted above. The rotation in the DJ Basin occurs slightly northeast of the RGR, within which S_{Hmax} is approximately north–south (Figure 1). It is also noteworthy that, where data are currently available, the rotation in the DJ Basin occurs approximately across the basin axis (Rocky Mountain Association of Geologists, 2014). In addition to these examples, Figure 1 shows that S_{Hmax} rotates markedly in southern Colorado and northern New Mexico, mostly in the Raton Basin, and in southeastern New Mexico and western Texas, in and near the Delaware subbasin of the Permian Basin. It is likely that more regions of variability may become evident along the margins of these extensional provinces as more S_{Hmax} orientations are collected and published.

Figure 9 takes a closer look at the complex stress fields in the Uinta-Piceance and DJ Basins. It is clear from this more detailed scale that S_{Hmax} orientations change systematically with location, with nearby measurements yielding similar S_{Hmax} orientations. The plots beside each map indicate mean S_{Hmax} orientations as a function of depth (with one standard deviation of variability) in the blue and black populations.

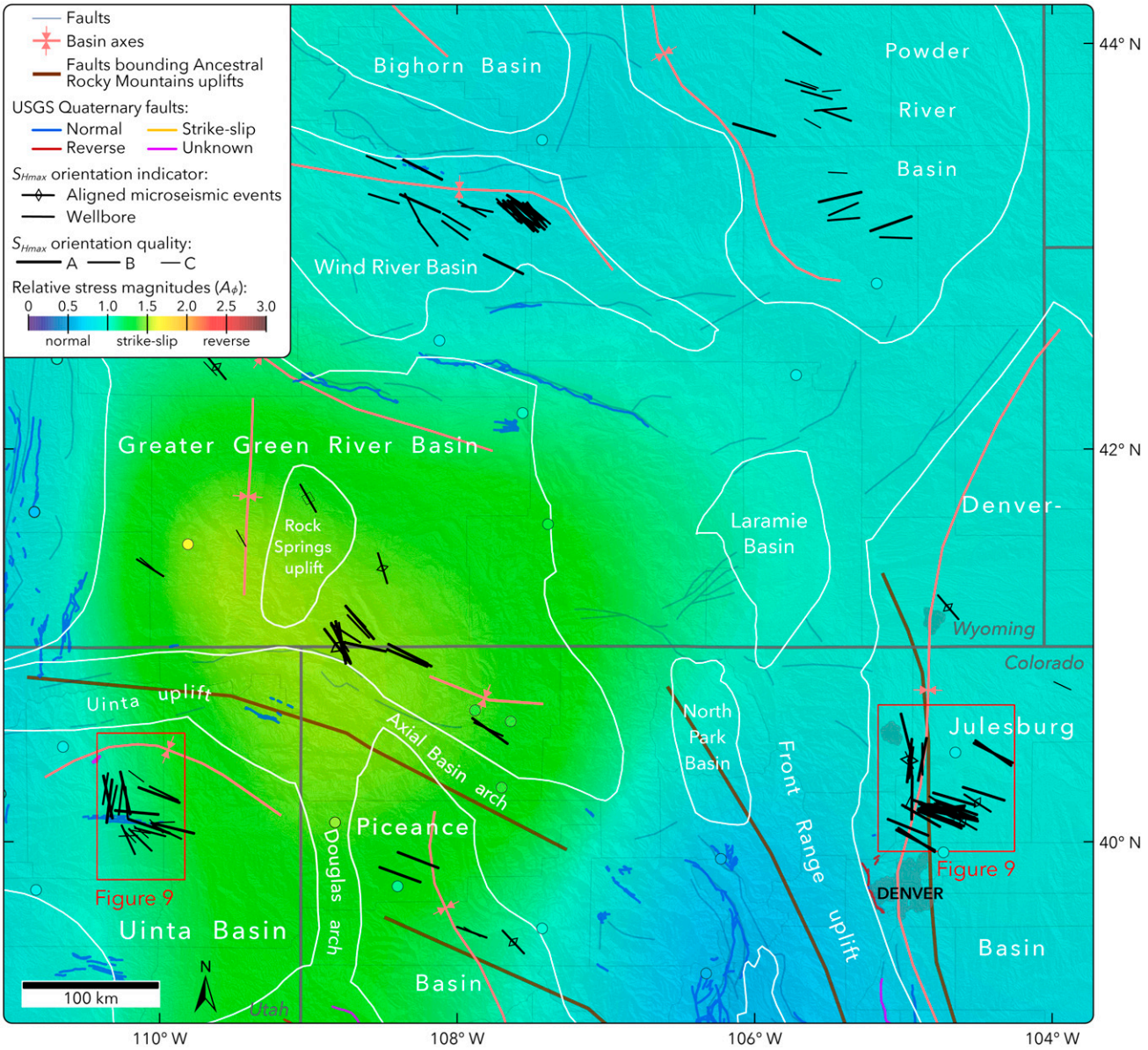

Figure 8. State of stress in Rocky Mountains basins, western United States. Nearly all maximum horizontal principal stress (S_{Hmax}) orientations in the Wind River Basin are from Thompson (2015), and most of the remaining S_{Hmax} orientations across this region are from Lund Snee and Zoback (2020a). Light blue faults are from Marshak et al. (2000) and Garrity and Soller (2009), and bold, brightly colored faults are from the US Geological Survey (USGS) Quaternary Faults and Folds Database (Crone and Wheeler, 2000). Selected basin outlines and axes are from the Rocky Mountain Association of Geologists (2014). See Figure 1 for map location.

These plots demonstrate that S_{Hmax} orientation does not vary with depth despite the pronounced horizontal variabilities. In fact, nearby focal mechanisms appear consistent with the measurements from the shallower basin sedimentary rocks (as shown for the DJ Basin in the right-hand panel of Figure 9), suggesting that these variations are significant at the scale of the brittle upper crust. It should be noted that the abrupt stress orientation changes in both areas shown in Figure 9 indicate approximately 90° changes in stress orientation, suggesting a switch between S_{hmin} and S_{Hmax}. Although the reason for the short spatial distances of these rotations is not yet established (see Lund Snee and Zoback, 2020a), if P_P is elevated such that the difference between S_{hmin} and S_{Hmax} is relatively small (see Figure 2), any process that might

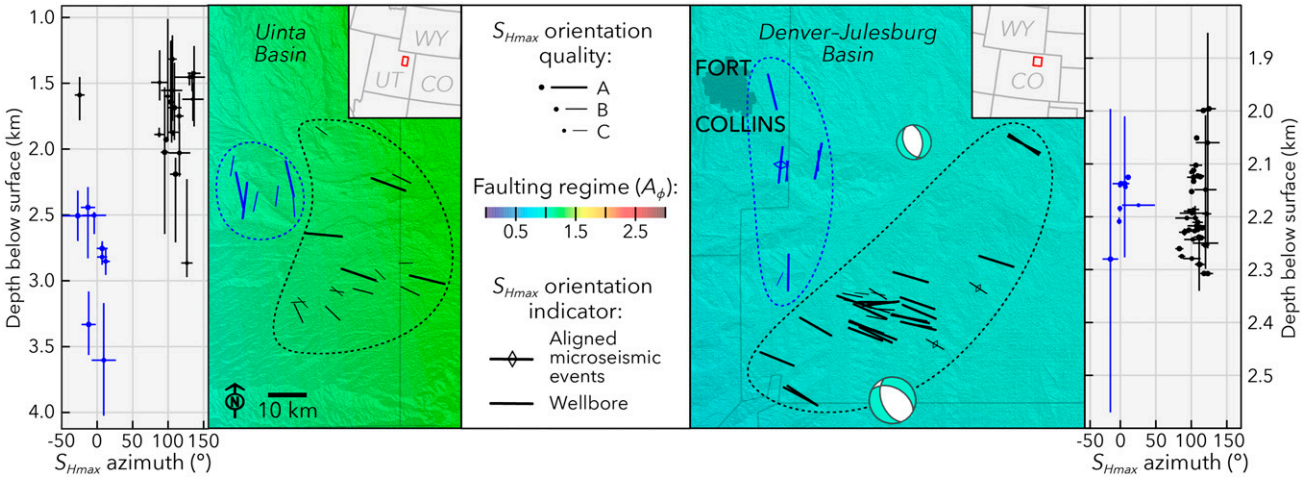

Figure 9. Maps showing short-wavelength rotations of maximum horizontal principal stress (S_{Hmax}) in the Uinta Basin, northeastern Utah (on the left), and the Denver-Julesburg Basin, northern Colorado (on the right). The orientation of S_{Hmax} changes markedly across these basins but does not rotate with depth. Maps are at the same scale. The vertical bars in the depth plots indicate the vertical span of stress indicators measured in wells, and the horizontal bars indicate one standard deviation of S_{Hmax} orientations. Focal mechanisms are from the compilation described in the text. A_ϕ = relative stress magnitudes.

increase S_{hmin} or decrease S_{Hmax} independently of the other could result in an ~90° change is horizontal stress orientations.

The short distance of these observed changes of stress orientations suggests shallow sources of stress, probably within the brittle crust. Crustal density anomalies are likely sources of stress, as suggested by the pronounced variabilities in Bouguer gravity anomaly in these areas (Kucks, 1999). In the case of the rotation mapped in the DJ Basin, geologic features that could provide sharp lateral density gradients include the margins of Carboniferous–Permian Ancestral Rocky Mountains uplifts, some of which were reactivated by Cretaceous–Paleogene thick-skinned shortening that occurred during the Laramide orogeny (Marshak et al., 2003). One of these features is located approximately along the axis of the mapped rotation in the DJ Basin. We also note that the rotation observed within the northern Uinta-Piceance Basin occurs across the Duchesne-Pleasant Valley fault system, a prominent network of east-west–striking faults that display Quaternary-age normal offsets (Crone and Wheeler, 2000). It is possible that geologically recent fault offset could have locally rotated S_{Hmax} in this area. This phenomenon has been observed elsewhere (Castillo and Zoback, 1994; Hickman et al., 2000). However, we note that the stress perturbations associated with fault slip are typically limited to relatively small areas around the causative faults. Because the rotations observed in Figure 8 may be regionally persistent (i.e., a transition from approximately north-northeast–south-southwest S_{Hmax} in the BRP to east-southeast–west-northwest to the east in the Uinta-Piceance Basin, and from approximately north–south in the RGR to east-southeast–west-northwest to the east in the DJ Basin), transient local stress rotations attributable to recent faulting appear less likely.

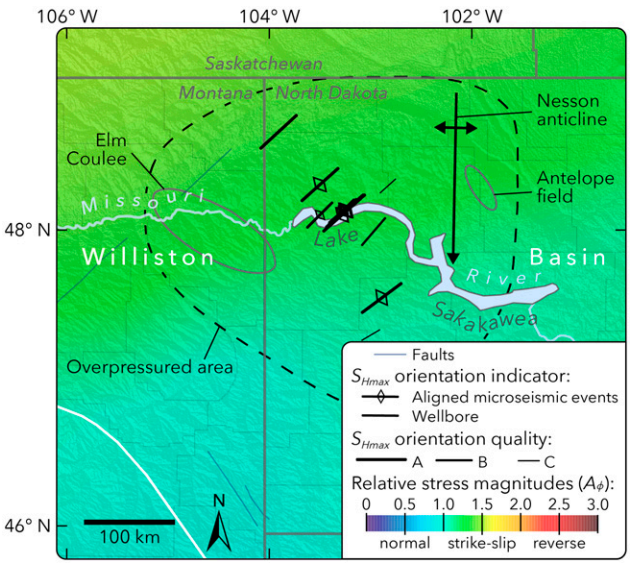

Figure 10. State of stress in the Williston Basin, eastern Montana, western South Dakota, and southeastern Saskatchewan. Basin outline and features are from Miller et al. (2008). See Figure 1 for map location. S_{Hmax} = maximum horizontal principal stress.

The Williston Basin, Eastern Montana, Western South Dakota, Southeastern Saskatchewan, and Southwestern Manitoba

Figure 10 shows the state of stress in the Williston Basin of northeastern Montana, northwestern North Dakota, southeastern Saskatchewan, and southwestern Manitoba. This region is a significant producer of oil and a relatively minor producer of gas (US Energy Information Administration, 2020). Production is dominantly from the thin (12–23 m) Upper Devonian–Lower Mississippian Bakken Formation, which consists of a middle siltstone member that is charged with oil by the organic-rich underlying lower and overlying upper "black shale" members (Nordquist, 1953; Meissner, 1991; Smith and Bustin, 2000; Miller et al., 2008; Kennedy et al., 2016). Some unconventional oil production also occurs from the underlying Late Devonian Three Forks Formation (Peale, 1893; Sandberg and Hammond, 1958; Miller et al., 2008).

Until recently, the only S_{Hmax} orientation available in this region was a single approximately northeast–southwest measurement published by Sturm and Gomez (2009), as well as a handful of

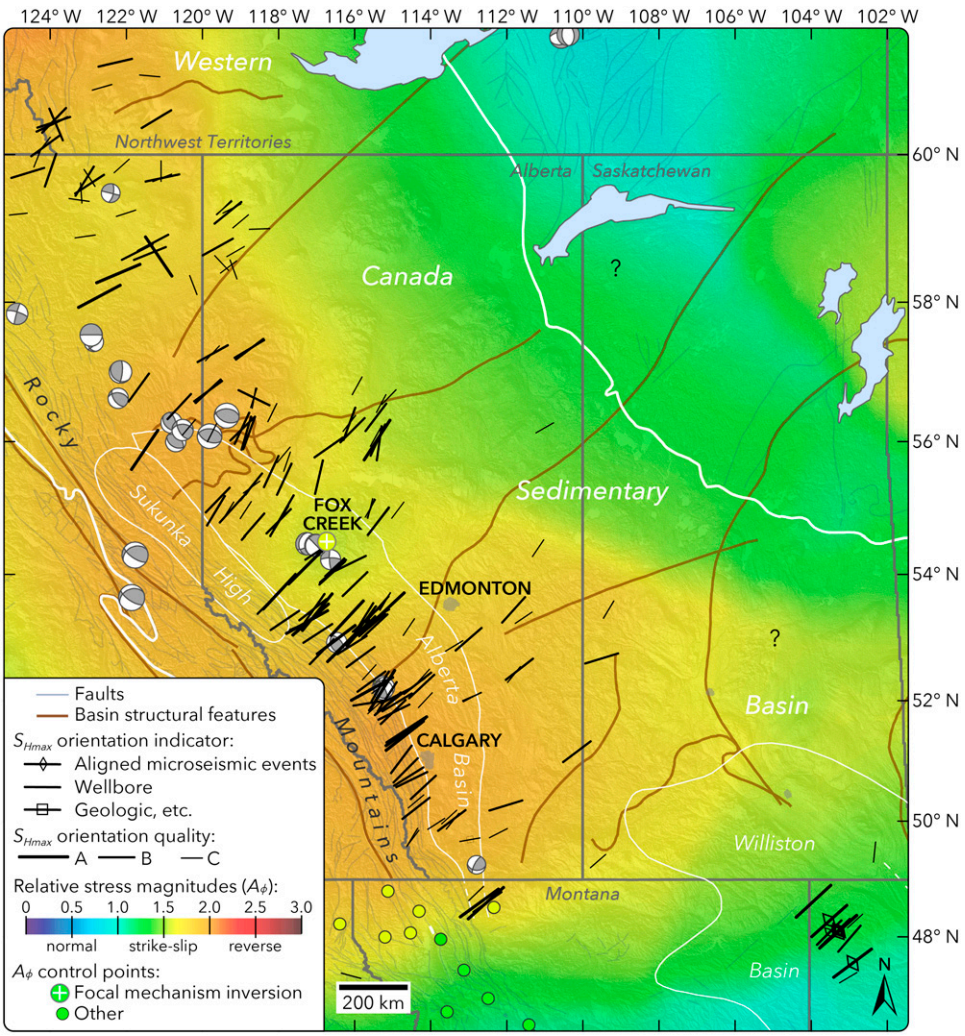

Figure 11. State of stress in the Western Canada Sedimentary Basin. Basin structural features, including basin and subdomain outlines, are from Wright et al. (1994). The Williston Basin outline is from Miller et al. (2008). See Figure 1 for map location. Focal mechanisms (from the compilation described in the text) are shown only in Canada to illustrate the compressive state of stress (SS–RF) in the Rocky Mountains and the crystalline basement farther east, and the less compressive (SS) faulting regime within the sedimentary succession of the basin (Fox Creek area). S_{Hmax} = maximum horizontal principal stress.

other published orientations that lacked sufficient information to meet the quality criteria. No measurements are currently recorded in the World Stress Map for this area. The S_{Hmax} orientation is quite consistently northeast–southwest within the central, strongly overpressured part of the play, around the western part of Lake Sakakawea in northwestern North Dakota (Figure 10). Interpreting A_ϕ estimates from earthquake focal mechanisms across the region (Figure 1), Lund Snee and Zoback (2020a) mapped a generally NF–SS stress state over the Williston Basin, transitioning gradually from nearly SS in southwestern Saskatchewan to NF–SS with NF dominant in northwestern South Dakota ($A_\phi < 1.0$). These estimates are supported by a NF–SS stress magnitude estimate by Yang and Zoback (2014) that is not included in the stress map because it is based on a single, poorly constrained focal plane mechanism.

The Western Canada Sedimentary Basin

The Western Canada Sedimentary Basin (WCSB), shown in Figure 11, is a major petroleum-producing region that contains numerous active tight oil and gas plays including the Middle and Upper Devonian Horn River and Muskwa Formations (e.g., Gal and Jones, 2003; Ross and Bustin, 2008; Ferri et al., 2011); the Upper Devonian Duvernay Formation (e.g., Andrichuk, 1958; Stoakes, 1980; Knapp et al., 2017); the Upper Devonian and Mississippian Bakken, Exshaw, and lower Banff Formations (e.g., Warren, 1937; Macqueen and Sandberg, 1970; Bustin et al., 1995; Smith and Bustin, 2000; Hartel et al., 2012); the Triassic Montney and Doig Formations (e.g., Davies et al., 1997; Dixon, 2000; Walsh et al., 2006); and several potential future plays (National Energy Board, 2011; Osadetz et al., 2018). The sedimentary system extends continuously from the southern Northwest Territories and southeastern Yukon Territories into the United States, where it includes basins in Montana, North Dakota, and Wyoming (e.g., the Williston and Powder River Basins). However, for convenience, the term WCSB typically refers only to the part in Canada, which encompasses the wedge of deformed Phanerozoic sedimentary rocks that spans from central British Columbia on the west to southwestern Manitoba on the east, including the Alberta Basin and a part of the Williston Basin, reaching a maximum thickness of ~6000 m in the deepest part of the Alberta Basin (e.g., Mossop and Shetsen, 1994; Wright et al., 1994).

As shown in Figure 11, the orientations of S_{Hmax} are well characterized in much of the WCSB, particularly in and near the Alberta Basin, largely because of contributions by Bell and Gough (1979) and Reiter et al. (2014). In general, S_{Hmax} is approximately northeast–southwest in the WCSB, including throughout most of the Alberta Basin, but it varies between east–west and north-northeast–south-southwest, depending on location. The S_{Hmax} orientations in northwestern Montana and northwestern South Dakota are also northeast–southwest (Lund Snee and Zoback, 2020a), consistent with those throughout the southern part of the WCSB. Figure 11 indicates a slight clockwise rotation northward from approximately northeast–southwest in northwestern Montana and southern Alberta to east-northeast–west-southwest or nearly east–west in the southern Northwest Territories and northeastern British Columbia. In addition, a slight counterclockwise rotation occurs eastward from the southern Alberta Basin to eastcentral Alberta and westcentral Saskatchewan, although S_{Hmax} remains broadly northeast–southwest across this area. The regional trends shown in Figure 1 indicate that S_{Hmax} likely remains oriented generally northeast–southwest to north-northeast–south-southwest between southern Alberta and western Ontario, outside the WCSB, despite the general sparsity of data in this region.

Absolute and relative magnitudes of the principal stresses are not as well constrained throughout the WCSB (Figure 11). Focal mechanisms along and slightly east of the Canadian Rockies suggest generally SS–RF (Ristau et al., 2007). However, in the Fox Creek area of westcentral Alberta, a focal mechanism stress inversion indicated a less compressive stress state of SS faulting (Zhang et al., 2019) within the sedimentary succession. Similarly, wellbore stress magnitude measurements from the Fox Creek area compiled by Shen et al. (2019) showed SS faulting ($S_{hmin} < S_V$). These patterns might indicate that the faulting regime is more compressive in the crystalline basement (SS–RF) than in the sedimentary succession (SS) in the Alberta Basin part of the WCSB.

The analysis by Shen et al. (2019) and prior work by Fox and Soltanzadeh (2015) showed that S_{hmin} within the sedimentary succession decreases gradually toward the northeast throughout westcentral Alberta, suggesting a slightly less compressive faulting regime in that direction. Broader regional trends inferred from focal mechanisms also suggest that the faulting regime becomes gradually less compressive eastward away from the SS–RF stress conditions in the crystalline basement near the Rocky Mountains, although focal mechanisms are almost completely absent between eastern Alberta and eastern Ontario. Legacy wellbore measurements compiled by Bell et al. (1994) suggested a similar eastward transition to a more extensional conditions, with SS or RF–SS slightly east of the Rockies transitioning to potentially NF farther east in southeastern Saskatchewan, but these data carried large uncertainties and were collected exclusively within the sedimentary succession.

CONCLUSIONS

We have presented detailed maps of the state of stress across the most active areas of unconventional energy development in North America. In most areas, these new maps represent the first quantitative description of the A_ϕ values (faulting regime), as well as their uncertainty ranges. As we have shown, the stress field varies coherently at multiple scales over these regions, even using several different measurement techniques. The data set employed several well-established methods for measuring S_{Hmax} orientation, largely from formal focal mechanism stress inversions and borehole image logs. We also presented two new techniques that have only recently become available, including measured orientations of legacy hydraulic fractures (from older development in vertical wells) that were intercepted by recent horizontal wells, as well as orientations of aligned microseismic events defining hydraulic fractures propagating during reservoir stimulation. Orientations of S_{Hmax} are typically very coherent with depth both in sedimentary basins and the underlying crystalline rock. However, in certain sedimentary rock types, the absolute and even relative (A_ϕ) stress magnitudes values may vary from tectonic conditions because of viscous stress relaxation. In addition, values of P_P that differ from hydrostatic can have profound effects on the maximum permissible differential stress magnitudes (Figure 2).

The data we have presented provide operators with tools to assist with improving operational efficiency for both unconventional and conventional development. Knowing the principal stress orientations and relative magnitudes enables operators to drill in the optimal direction, to predict which subset of preexisting fractures are likely to slip and form an interconnected permeable fracture network during reservoir stimulation, and to allow both operators and regulators to identify potentially active faults.

These new-generation stress maps of S_{Hmax} orientations and the quantitative representation of the relative stress magnitudes that are presented using the A_ϕ parameter for the first time provide the full relative stress tensor at any location. As we have shown, these data, together with additional information, can be used to approximate the magnitudes of S_{hmin} (approximately the fracture gradient in areas where NF or SS are dominant) and S_{Hmax}. Continued addition of data over the next few years from energy development and improved earthquake focal mechanism catalogs will provide increasingly tight constraints on the absolute magnitudes of the horizontal principal stresses.

APPENDIX 1 STRESS MEASUREMENT QUALITY CRITERIA

STRESS INDICATOR*		A	B	C
Drilling-induced tensile fractures		Ten or more distinct tensile fractures in a single well with sd $\leq 12^\circ$ and with highest and lowest observations at least 300 m apart	At least six distinct tensile fractures in a single well with sd $\leq 20^\circ$ and with highest and lowest observations at least 100 m apart	At least four distinct tensile fractures in a single well with sd $\leq 25^\circ$ and with highest and lowest observations at least 30 m apart
Focal mechanism inversions	Directions	Formal inversion of ≥ 35 reasonably well-constrained focal mechanisms resulting in stress directions with sd $\leq 12^\circ$	Formal inversion of ≥ 25 reasonably well-constrained focal mechanisms resulting in stress directions with sd $\leq 20^\circ$	Formal inversion of ≥ 20 reasonably well-constrained focal mechanisms resulting in stress directions with sd $\leq 25^\circ$
	Relative magnitude, ϕ or A_ϕ	Formal inversion of ≥ 35 reasonably well-constrained focal mechanisms resulting in ϕ with sd ≤ 0.05	Formal inversion of ≥ 25 reasonably well-constrained focal mechanisms resulting in ϕ with sd ≤ 0.1	Formal inversion of ≥ 20 reasonably well-constrained focal mechanisms resulting in ϕ with sd ≤ 0.2
Wellbore breakouts		Ten or more distinct breakout zones in a single well (or breakouts in two or more wells in close proximity) with sd $\leq 12^\circ$ and with highest and lowest observations at least 300 m apart	At least six distinct breakout zones in a single well with sd $\leq 20^\circ$ and with highest and lowest observations at least 100 m apart	At least four distinct breakout zones in a single well with sd $\leq 25^\circ$ and with highest and lowest observations at least 30 m apart
Hydraulic fractures	Openhole hydraulic fracturing stress orientation (HF)	Four or more hydraulic fractures in a single well (or average of HFs for two or more wells in close geographic proximity) with sd $\leq 12^\circ$	Three or more hydraulic fractures in a single well (or average of HFs for two or more wells in close geographic proximity) with sd $\leq 20^\circ$	Two or more HFs in a single well with 20° sd $\leq 25^\circ$. If a distinct orientation change with depth, the deepest measurements assumed valid
	Hydraulic fractures observed in nearby subhorizontal wellbores	Twelve or more distinct hydraulic fractures in a single well (or average of HFs for two or more wells in close geographic proximity) with sd $\leq 12^\circ$	Three or more hydraulic fractures in a single well (or average of HFs for two or more wells in close geographic proximity) with sd $\leq 20^\circ$.	Six or more distinct hydraulic fractures in a single well (or average of HFs for two or more wells in close geographic proximity) with sd $\leq 25^\circ$
	Microseismic alignments along hydraulic fractures	Twelve or more distinct linear zones associated with HF stages, with sd $\leq 12^\circ$	Eight or more distinct linear zones associated with HF stages, with sd $\leq 20^\circ$	Six or more distinct linear zones associated with HF stages, with sd $\leq 25^\circ$
Shear velocity anisotropy from crossed-dipole logs†		Anisotropy $\geq$ 2% present at a consistent azimuth, with highest and lowest observations at least 300 m apart, and with sd of fast azimuth $\leq 12^\circ$	Anisotropy $\geq$ 2% present at a consistent azimuth, with highest and lowest observations at least 100 m apart, and with sd of fast azimuth $\leq 20^\circ$	Anisotropy $\geq$ 2% present at a consistent azimuth, with highest and lowest observations at least 30 m apart, and with sd of fast azimuth $\leq 25^\circ$

Abbreviation: sd = standard deviation.

*For all indicators except for hydraulic fractures induced and measured in open holes (HF), the shallowest measurement must be at least 100 m deep and also sufficiently deep that measurements are not affected by topography. For open-hole HFs, the shallowest measurement must be ≥300 m depth.

†In addition to anisotropy ≥2%, measurements should ideally have an energy difference between fast and slow shear waves ≥50% and a minimum energy ≥15%.

APPENDIX 2. EQUATIONS RELATING A_ϕ TO STRESS MAGNITUDES

This appendix provides the equations that relate relative stress magnitudes A_ϕ to absolute stress magnitudes in NF, SS, and RF regimes, after Lund Snee (2020). For reasons given in the main text, the equations assume that values of S_V, P_P, and the coefficient of friction (μ) are known or can be reasonably estimated. Typically, S_V is the easiest and least expensive stress magnitude to measure, so the equations below illustrate how S_{Hmax} and S_{hmin} can be estimated assuming values of S_V and P_P. Here it is assumed that $\mu = 0.6$.

Determining the bounding magnitudes of S_{Hmax} and S_{hmin} commonly requires the assumption that the crust is in a state of frictional failure equilibrium, as is done in Figure 2. Figure 2 also illustrates the significance of P_P for determining the limiting stress magnitudes. The upper panel of Figure 2 shows the case of approximately hydrostatic P_P, whereas the lower panel shows the case of significant overpressure.

In general, it is likely that the latter condition of significant overpressure is more relevant for most areas where unconventional oil and gas are developed. Compilations of wellbore measurements have shown extremely high P_P values in many of these areas, including parts of the Delaware subbasin of western Texas and southeastern New Mexico (Rittenhouse et al., 2016) and the Utica shale play (Figure 3) of the central and eastern United States (Patchen and Carter, 2015). As shown in Figure 2, higher P_P reduces the permissible differences between the principal stresses relative to S_V.

The A_ϕ parameter of Simpson (1997) was defined above in equation 1, but it is repeated here for clarity:

$$A_\phi = (n + 0.5) + (-1)^n(\phi - 0.5) \tag{4}$$

where

$$\phi = \frac{S_2 - S_3}{S_1 - S_3} = 1 - R \tag{5}$$

and where R is the shape ratio (another parameter that is commonly used for expressing relative stress magnitudes), $n = 0$ for NF ($0 \le A_\phi \le 1.0$), $n = 1$ for SS ($1.0 \le A_\phi \le 2.0$), and $n = 2$ for RF ($2.0 \le A_\phi \le 3.0$). For some applications, it is helpful to first reorder equation 4 in terms of ϕ:

$$\phi = \frac{A_\phi - n - 0.5}{(-1)^n} + 0.5 \tag{6}$$

To abide by the assumption of frictional failure equilibrium, it is assumed here that the differential effective stresses, σ_{ii}, are approximately at the Mohr-Coulomb frictional failure limit. As also given in equation 3, the frictional stress limits are expressed as

$$\frac{\sigma_1}{\sigma_3} = \frac{S_1 - P_P}{S_3 - P_P} = [(\mu^2 + 1)^{1/2} + \mu]^2 \approx 3.12 \tag{7}$$

after Jaeger et al. (2007).

As is evident from equations 5, 6, and 7, the equations relating A_ϕ to principal stress magnitudes vary depending upon the style of faulting because the faulting regime determines which principal stresses correspond to S_1, S_2, and S_3. For NF,

$$n = 0, \tag{8}$$

$$S_1 = S_V = \rho g Z, \text{ or } \int_{z=0}^{Z} \rho(z) g \, dz, \leftarrow \textit{definition of vertical stress} \tag{9}$$

$$S_3 = S_{hmin} = \frac{S_V - P_P}{3.12} + P_P, \leftarrow \textit{from equation 7} \tag{10}$$

$$S_2 = S_{Hmax} = A_\phi(S_V - S_{hmin}) + S_{hmin}$$
$$= \phi(S_V - S_{hmin}) + S_{hmin}, \leftarrow \textit{from equations 4 and 5} \tag{11}$$

where z is depth and Z is the depth of interest. The case of SS is more involved:

$$n = 1, \tag{12}$$

$$S_2 = S_V = \int_{z=0}^{Z} \rho(z) g \, dz, \tag{13}$$

$$S_3 = S_{hmin} = \frac{S_{Hmax} - P_P}{3.12} + P_P, \tag{14}$$

$$S_1 = S_{Hmax} = \frac{S_V - S_{hmin}}{\phi} + S_{hmin}$$
$$= \frac{1}{\phi}\left(S_V - \left[\frac{S_{Hmax} - P_P}{3.12} + P_P\right]\right) + \left[\frac{S_{Hmax} - P_P}{3.12} + P_P\right]$$
$$= \frac{1}{\phi}S_V - \frac{1}{3.12\phi}(S_{Hmax} - P_P)$$
$$- \frac{1}{\phi}P_P + \frac{1}{3.12}(S_{Hmax} - P_P) + P_P \tag{15}$$

$$S_{Hmax} + (S_{Hmax} - P_P)\left(\frac{1}{3.12\phi} - \frac{1}{3.12}\right) = \frac{1}{\phi}S_V - \frac{1}{\phi}P_P + P_P \tag{16}$$

$$S_{Hmax} = \frac{\frac{1}{\phi}S_V - \frac{1}{\phi}P_P + P_P + P_P\left(\frac{1}{3.12\phi} - \frac{1}{3.12}\right)}{1 + \frac{1}{3.12\phi} - \frac{1}{3.12}}$$

$$= \frac{\frac{1}{2-A_\phi}S_V - \frac{1}{2-A_\phi}P_P + P_P + P_P\left(\frac{1}{3.12(2-A_\phi)} - \frac{1}{3.12}\right)}{1 + \frac{1}{3.12(2-A_\phi)} - \frac{1}{3.12}}. \tag{17}$$

Finally, for RF,

$$n = 2, \tag{18}$$

$$S_3 = S_V = \int_{z=0}^{Z} \rho(z) g \, dz, \tag{19}$$

$$S_1 = S_{Hmax} = 3.12(S_V - P_P) + P_P, \quad (20)$$

$$S_2 = S_{hmin} = \phi(S_{Hmax} - S_V) + S_V = (A_\phi - 2)(S_{Hmax} - S_V) + S_V. \quad (21)$$

It bears repeating that these equations provide the bounding limits of the minimum and maximum principal stress magnitudes, but the actual magnitudes of S_{Hmax} and S_{hmin} may fall between these limits for a given value of A_ϕ, particularly within rocks that have experienced viscous stress relaxation. However, the value of S_V is fixed because it is imposed by the weight of the overburden.

REFERENCES CITED

Alalli, A. A., and M. D. Zoback, 2018, Microseismic evidence for horizontal hydraulic fractures in the Marcellus Shale, southeastern West Virginia: Leading Edge, v. 37, no. 5, p. 356–361, doi:10.1190/tle37050356.1.

Alt, R. C., and M. D. Zoback, 2017, In situ stress and active faulting in Oklahoma: Bulletin of the Seismological Society of America, v. 107, no. 1, p. 216–228, doi:10.1785/0120160156.

Anderson, E. M., 1951, The dynamics of faulting and Dyke Formation with applications to Britain: Edinburgh and London, Oliver and Boyd, 206 p.

Andrichuk, J. M., 1958, Cooking Lake and Duvernay (Late Devonian) sedimentation in Edmonton area of central Alberta, Canada: AAPG Bulletin, v. 42, no. 9, p. 2189–2222, doi:10.1306/0BDA5BB5-16BD-11D7-8645000102C1865D.

Angelier, J., 1979, Determination of the mean principal directions of stresses for a given fault population: Tectonophysics, v. 56, no. 3–4, p. T17–T26, doi:10.1016/0040-1951(79)90081-7.

Bell, J. S., and D. I. Gough, 1979, Northeast-southwest compressive stress in Alberta: Evidence from oil wells: Earth and Planetary Science Letters, v. 45, no. 2, p. 475–482, doi:10.1016/0012-821X(79)90146-8.

Bell, J. S., P. R. Price, and P. J. McLellan, 1994, In-situ stress in the Western Canada sedimentary basin, *in* G. D. Mossop and I. Shetsen, eds., Geological atlas of the Western Canada Sedimentary Basin: Calgary, Canada, Canadian Society of Petroleum Geologists and Alberta Research Council, p. 439–446.

Blackwell, D. D., M. C. Richards, Z. S. Frone, J. F. Batir, M. A. Williams, A. A. Ruzo, R. K. Dingwall, and M. Williams, 2011, Temperature at depth maps for the conterminous US and geothermal resource estimates (GRC1029452): GRC Transactions, v. 35, p. 1545–1550.

Bowker, K. A., 2003, Recent developments of the Barnett Shale play, Fort Worth basin: West Texas Geological Society Bulletin, v. 42, no. 6, p. 4–11.

Bowker, K. A., 2007, Barnett Shale gas production, Fort Worth Basin: Issues and discussion: AAPG Bulletin, v. 91, no. 4, p. 523–533, doi:10.1306/06190606018.

Braunmiller, J., and J. Nábělek, 2002, Seismotectonics of the Explorer region: Journal of Geophysical Research: Solid Earth, v. 107, no. B10, p. ETG 1-1–ETG 1-25, doi:10.1029/2001JB000220.

Bustin, R. M., M. G. Smith, and M. L. Caplan, 1995, Sequence stratigraphy of the Bakken and Exshaw Formations: A continuum of black shale formations in the Western Canada sedimentary basin: Seventh International Williston Basin Symposium, Billings, Montana, July 23–25, 1995, p. 399–409.

Byerlee, J. D., 1978, Friction of rocks: Pure and Applied Geophysics, v. 116, no. 4–5, p. 615–626, doi:10.1007/BF00876528.

Cardott, B. J., 2012, Thermal maturity of Woodford Shale gas and oil plays, Oklahoma, USA: International Journal of Coal Geology, v. 103, p. 109–119, doi:10.1016/j.coal.2012.06.004.

Castillo, D. A., and M. D. Zoback, 1994, Systematic variations in stress state in the southern San Joaquin Valley: Inferences based on well-bore data and contemporary seismicity: AAPG Bulletin, v. 78, no. 8, p. 1257–1275, doi:10.1306/A25FEAC7-171B-11D7-8645000102C1865D.

Crone, A. J., and K. V. Luza, 1990, Style and timing of Holocene surface faulting on the Meers fault, southwestern Oklahoma: Bulletin of the Geological Society of America, v. 102, no. 1, p. 1–17, doi:10.1130/0016-7606(1990)102<0001:SATOHS>2.3.CO;2.

Crone, A. J., and R. L. Wheeler, 2000, Data for Quaternary faults, liquefaction features, and possible tectonic features in the Central and Eastern United States, east of the Rocky Mountain front: Washington, DC, US Geological Survey Open-File Report 00-260, 342 p., doi:10.3133/ofr00260.

Curtis, J. B., 2002, Fractured shale-gas systems: AAPG Bulletin, v. 86, no. 11, p. 1921–1938, doi:10.1306/61EEDDBE-173E-11D7-8645000102C1865D.

Darold, A. P., and A. A. Holland, 2015, Preliminary Oklahoma optimal fault orientations: Norman, Oklahoma, Oklahoma Geological Survey Open File Report OF4-2015.

Davies, G. R., T. F. Moslow, and M. D. Sherwin, 1997, The lower Triassic Montney Formation, west-central Alberta: Bulletin of Canadian Petroleum Geology, v. 45, no. 4, p. 474–505.

Decker, C. E., 1933, Viola limestone, primarily of Arbuckle and Wichita mountain regions, Oklahoma: AAPG Bulletin, v. 17, no. 12, p. 1405–1435.

Dixon, J., 2000, Regional lithostratigraphic units in the Triassic Montney Formation of western Canada: Bulletin of Canadian Petroleum Geology, v. 48, no. 1, p. 80–83, doi:10.2113/48.1.80.

Dziewoński, A. M., T.-A. Chou, and J. H. Woodhouse, 1981, Determination of earthquake source parameters from waveform data for studies of global and regional seismicity: Journal of Geophysical Research. Solid Earth, v. 86, no. B4, p. 2825–2852, doi:10.1029/JB086iB04p02825.

Eaton, D. W., and A. B. Mahani, 2015, Focal mechanisms of some inferred induced earthquakes in Alberta, Canada: Seismological Research Letters, v. 86, no. 4, p. 1078–1085, doi:10.1785/0220150066.

Ekström, G., M. Nettles, and A. M. Dziewoński, 2012, The global CMT project 2004-2010: Centroid-moment tensors for 13,017 earthquakes: Physics of the Earth and Planetary Interiors, v. 200–201, p. 1–9, doi:10.1016/j.pepi.2012.04.002.

Evans, K. F., 1989, Appalachian stress study: 3. Regional scale stress variations and their relation to structure and contemporary tectonics: Journal of Geophysical Research, v. 94, no. B12, p. 17619, doi:10.1029/JB094iB12p17619.

Ewing, T. E., R. T. Budnik, J. T. Ames, and D. M. Ridner, 1990, Tectonic map of Texas: Austin, Texas, Bureau of Economic Geology, University of Texas at Austin, scale 1:750,000, 4 sheets.

Ewing, T. E., and R. F. Lopez, 1991, Principal structural features, Gulf of Mexico basin, *in* A. Salvador, ed., The Gulf of Mexico Basin: The geology of North America v. J: Boulder, Colorado, Geological Society of America, plate 2, 1 sheet.

Ferri, F., A. S. Hickin, and D. H. Huntley, 2011, Besa River Formation, western Liard basin, British Columbia (NTS 094N): Geochemistry and regional correlations: Vancouver, Canada, British Columbia Ministry of Energy and Mines Geoscience Reports, 18 p.

Fisher, K., and N. Warpinski, 2012, Hydraulic-fracture-height growth: Real data: SPE Production & Operations, v. 27, no. 1, p. 8–19, doi:10.2118/145949-PA.

Forand, D., V. Heesakkers, and K. Schwartz, 2017, Constraints on natural fracture and in-situ stress trends of unconventional reservoirs in the Permian Basin, USA: Unconventional Resources Technology Conference, Austin, Texas, July 24–26, 2017, p. 654–672, doi:10.15530/URTEC-2017-2669208.

Fox, A. D., and M. Soltanzadeh, 2015, A regional geomechanical study of the Duvernay Formation in Alberta, Canada: Proceedings of GeoConvention 2015: New Horizons, Calgary, Canada, May 4–8, 2015, 4 p.

Freeman, T., 1964, Algal limestones of the Marble Falls Formation (Lower Pennsylvanian), central Texas: Bulletin of the Geological Society of America, v. 75, no. 7, p. 669–676, doi:10.1130/0016-7606(1964)75[669:ALOTMF]2.0.CO;2.

Friedman, M., and H. C. Heard, 1974, Principal stress ratios in Cretaceous limestones from Texas Gulf Coast: AAPG Bulletin, v. 58, no. 1, p. 71–78, doi:10.1306/83D9137B-16C7-11D7-8645000102C1865D.

Gal, L. P., and A. L. Jones, 2003, Oil and gas potential evaluation of the Deh Cho territory: Yellowknife, Canada, Northwest Territories Open File 2003-03, 88 p.

Gale, J. F. W., R. M. Reed, and J. Holder, 2007, Natural fractures in the Barnett Shale and their importance for hydraulic fracture treatments: AAPG Bulletin, v. 91, no. 4, p. 603–622, doi:10.1306/11010606061.

Garrity, C. P., and D. R. Soller, 2009, Database of the geologic map of North America: Adapted from the map by J.C. Reed, Jr. and others (2005): Washington, DC, US Geological Survey Data Series 424, 10 p., doi:10.3133/ds424.

Gaswirth, S. B., K. L. French, J. K. Pitman, K. R. Marra, T. J. Mercier, H. M. Leathers-Miller, C. J. Schenck, et al., 2018, Assessment of undiscovered continuous oil and gas resources in the Wolfcamp shale and Bone Spring Formation of the Delaware basin, Permian Basin Province, New Mexico and Texas, 2018: Washington, DC, US Geological Survey Fact Sheet 2018–3073, 4 p., 10.3133/fs20183073.

Gaswirth, S. B., K. R. Marra, P. G. Lillis, T. J. Mercier, H. M. Leathers-Miller, C. J. Schenck, T. R. Klett, et al., 2016, Assessment of undiscovered continuous oil resources in the Wolfcamp shale of the Midland basin, Permian Basin Province, Texas, 2016: Washington, DC, US Geological Survey Fact Sheet 2016-3092, 4 p., 10.3133/fs20163092.

Green, G. N., and G. E. Jones, 1997, The digital geologic map of New Mexico in ARC/INFO format: Washington, DC, US Geological Survey Open File Report 97–52, 9 p., doi:10.3133/ofr9752.

Haimson, B. C., 1977, Crustal stress in the continental United States as derived from hydrofracturing tests, *in* J. G. Heacock, G. V. Keller, J. E. Oliver, and G. Simmons, eds., The Earth's crust: Washington, DC: American Geophysical Union Monograph Series 20, p. 576–592, doi:10.1029/GM020p0576.

Hakso, A., and M. D. Zoback, 2019, The relation between stimulated shear fractures and production in the Barnett shale: Implications for unconventional oil and gas reservoirs: Geophysics, v. 84, no. 6, p. B461–B469, doi:10.1190/geo2018-0545.1.

Harris, S. A., 1975, Hydrocarbon accumulation in "Meramec-Osage" (Mississippian) rocks, Sooner trend, northwest-central Oklahoma: AAPG Bulletin, v. 59, no. 4, p. 633–664, doi:10.1306/83D91CF4-16C7-11D7-8645000102C1865D.

Hartel, T. H. D., B. C. Richards, and C. W. Langenberg, 2012, Wabamun, Bakken-equivalent Exshaw, and Banff formations in core, cuttings, and outcrops from southern Alberta: AAPG Search and Discovery article 50952, accessed August 30, 2020, https://www.searchanddiscovery.com/pdfz/documents/2017/50952hartel/ndx_hartel.pdf.html.

Hauksson, E., W. Yang, and P. M. Shearer, 2012, Waveform relocated earthquake catalog for Southern California (1981 to June 2011): Bulletin of the Seismological Society of America, v. 102, no. 5, p. 2239–2244, doi:10.1785/0120120010.

Hawkins, S. J., R. R. Charpentier, C. J. Schenk, H. M. Leathers-Miller, T. R. Klett, M. E. Brownfield, T. M. Finn, et al., 2016, Assessment of continuous (unconventional) oil and gas resources in the Late Cretaceous Mancos Shale of the Piceance basin, Uinta-Piceance Province, Colorado and Utah, 2016: Washington, DC, US Geological Survey Fact Sheet 2016-3030, 4 p., doi:10.3133/fs20163030.

Heidbach, O., M. Rajabi, X. Cui, K. Fuchs, B. Müller, J. Reinecker, K. Reiter, et al., 2018, The World Stress Map database release 2016: Crustal stress pattern across scales: Tectonophysics, v. 744, p. 484–498, doi:10.1016/j.tecto.2018.07.007.

Hennings, P. H., J.-E. Lund Snee, J. L. Osmond, H. R. DeShon, R. Dommisse, E. Horne, C. Lemons, and M. D.

Zoback, 2019, Injection-induced seismicity and fault-slip potential in the Fort Worth basin, Texas: Bulletin of the Seismological Society of America, v. 109, no. 5, p. 1615–1634, doi:10.1785/0120190017.

Herrmann, R. B., H. M. Benz, and C. J. Ammon, 2011, Monitoring the earthquake source process in North America: Bulletin of the Seismological Society of America, v. 101, no. 6, p. 2609–2625, doi:10.1785/0120110095.

Hickman, S. H., M. D. Zoback, C. A. Barton, R. Benoit, J. Svitek, and R. Summers 2000, Stress and permeability heterogeneity within the Dixie Valley geothermal reservoir: Recent results from well 82-5: 25th Workshop on Geothermal Reservoir Engineering, Stanford, California, January 24–26, 2000, p. 256–265.

Higley, D. K., T. A. Cook, R. M. Pollastro, R. R. Charpentier, T. R. Klett, and J. W. Schmoker, 2007, Executive summary—2002 Assessment of undiscovered oil and gas in the Denver Basin Province, Colorado, Kansas, Nebraska, South Dakota, and Wyoming, *in* Petroleum systems and assessment of undiscovered oil and gas in the Denver Basin Province, Colorado, Kansas, Nebraska, South Dakota, and Wyoming—USGS Province 39: Washington, DC, US Geological Survey Digital Data Series DDS–69–P:, 4 p.

Hurd, O., and M. D. Zoback, 2012, Intraplate earthquakes, regional stress and fault mechanics in the central and eastern U.S. and southeastern Canada: Tectonophysics, v. 581, p. 182–192, doi:10.1016/j.tecto.2012.04.002.

Ichinose, G. A., J. G. Anderson, K. D. Smith, and Y. Zeng, 2003, Source parameters of eastern California and western Nevada earthquakes from regional moment tensor inversion: Bulletin of the Seismological Society of America, v. 93, no. 1, p. 61–84, doi:10.1785/0120020063.

Ingersoll, R. V., 2001, Structural and stratigraphic evolution of the Rio Grande rift, northern New Mexico and southern Colorado: International Geology Review, v. 43, no. 10, p. 867–891, doi:10.1080/00206810109465053.

Jaeger, J. C., N. G. W. Cook, and R. W. Zimmerman, 2007, Fundamentals of rock mechanics, 4th ed.: Oxford, United Kingdom, Blackwell Publishing Ltd., 488 p.

Jarvie, D. M., R. J. Hill, T. E. Ruble, and R. M. Pollastro, 2007, Unconventional shale-gas systems: The Mississippian Barnett Shale of north-central Texas as one model for thermogenic shale-gas assessment: AAPG Bulletin, v. 91, no. 4, p. 475–499, doi:10.1306/12190606068.

Johnson, R. C., J. E. Birdwell, T. J. Mercier, and M. E. Brownfield, 2016, Geology of tight oil and potential tight oil reservoirs in the Lower Part of the Green River Formation, Uinta, Piceance, and Greater Green River basins, Utah, Colorado, and Wyoming: Washington, DC, US Geological Survey Scientific Investigations Report 2016-5008, 75 p., doi:10.3133/sir20165008.

Johnson, R. C., T. J. Mercier, M. E. Brownfield, and J. G. Self, 2011, Assessment of in-place oil shale resources in the Eocene Green River Formation, Uinta Basin, Utah and Colorado: Washington, DC, US Geological Survey Digital Data Series DDS-69-BB, 153 p., doi:10.3133/fs20103010.

Kao, H., and P.-R. Jian, 1999, Source parameters of regional earthquakes in Taiwan: July 1995–December 1996: Diqiu Kexue Jikan, v. 10, no. 3, p. 585, doi:10.3319/TAO.1999.10.3.585(T).

Kao, H., P.-R. Jian, K.-F. Ma, B.-S. Huang, and C.-C. Liu, 1998, Moment-tensor inversion for offshore earthquakes east of Taiwan and their implications to regional collision: Geophysical Research Letters, v. 25, no. 19, p. 3619–3622, doi:10.1029/98GL02803.

Kao, H., S.-J. Shan, A. Bent, C. Woodgold, G. Rogers, J. F. Cassidy, and J. Ristau, 2012, Regional centroid-moment-tensor analysis for earthquakes in Canada and adjacent regions: An update: Seismological Research Letters, v. 83, no. 3, p. 505–515, doi:10.1785/gssrl.83.3.505.

Kennedy, R., L. X. Luo, and V. Kusskra, 2016, The unconventional basins and plays—North America, the rest of the world and emerging basins, *in* U. Ahmed and D. N. Meehan, eds., Unconventional oil and gas resources: Exploitation and development: Boca Raton, Florida, CRC Press, p. 4-1–4-34, doi:10.1201/b20059-5.

King, P. B., and R. E. King, 1929, Stratigraphy of outcropping Carboniferous and Permian rocks of Trans-Pecos Texas: AAPG Bulletin, v. 13, no. 8, p. 907–926, doi:10.1306/3D93286B-16B1-11D7-8645000102C1865D.

Kirschbaum, M. A., C. J. Schenk, T. A. Cook, R. T. Ryder, R. R. Charpentier, T. R. Klett, S. B. Gaswirth, M. E. Tennyson, and K. J. Whidden, 2012, Assessment of undiscovered oil and gas resources of the Ordovician Utica shale of the Appalachian Basin Province, 2012: US Geological Survey Fact Sheet 2012-3116, 6 p.

Knapp, L. J., J. M. McMillan, and N. B. Harris, 2017, A depositional model for organic-rich Duvernay Formation mudstones: Sedimentary Geology, v. 347, p. 160–182, doi:10.1016/j.sedgeo.2016.11.012.

Kucks, R. P., 1999, Bouguer gravity anomaly data grid for the conterminous US, *in* J. D. Phillips, J. S. Duval, and R. A. Ambroziak, eds., National geophysical data grids; gamma-ray, gravity, magnetic and topographic data for the conterminous United States: Washington, DC, US Geological Survey Digital Data Series DDS-9, accessed August 30, 2020, https://mrdata.usgs.gov/gravity/bouguer/.

Lachenbruch, A. H., and J. H. Sass, 1980, Heat flow and energetics of the San Andreas fault zone: Journal of Geophysical Research: Solid Earth, v. 85, no. B11, p. 6185–6222, doi:10.1029/JB085iB11p06185.

Lockner, D., C. Morrow, D. Moore, and S. Hickman, 2011, Low strength of deep San Andreas fault gouge from SAFOD core: Nature, v. 472, no. 7341, p. 82–85, doi:10.1038/nature09927.

Lund, K., S. E. Box, C. Holm-Denoma, C. A. San Juan, R. J. Blakely, R. W. Saltus, E. D. Anderson, and E. H. Dewitt, 2015, Basement domain map of the conterminous United States and Alaska: Washington, DC, US Geological Survey Data Series 898, 48 p., doi:10.3133/ds898.

Lund Snee, J.-E., 2020, State of stress in North America: Seismicity, tectonics, and unconventional energy development, Ph.D. thesis, Stanford University, Stanford, California, 254 p., doi:10.13140/RG.2.2.27217.07523/1.

Lund Snee, J.-E., and N. Z. Dvory, 2020, Magnitude 5.0 earthquake shakes west Texas, accessed March 10, 2021, https://www.jenseriklundsnee.com/blog/2020/3/27/magnitude-50-earthquake-shakes-west-texas.

Lund Snee, J.-E., and M. D. Zoback, 2016, State of stress in Texas: Implications for induced seismicity: Geophysical Research Letters, v. 43, no. 19, p. 10,208–10,214, doi:10.1002/2016GL070974.

Lund Snee, J.-E., and M. D. Zoback, 2018, State of stress in the Permian basin, Texas and New Mexico: Implications for induced seismicity: Leading Edge, v. 37, no. 2, p. 127–134, doi:10.1190/tle37020127.1.

Lund Snee, J.-E., and M. D. Zoback, 2020a, Multiscale variations of the crustal stress field throughout North America: Nature Communications, v. 11, p. 1951, doi:10.1038/s41467-020-15841-5.

Lund Snee, J.-E., and M. D. Zoback, 2020b, State of stress and seismotectonics in the vicinity of the August 9, 2020 M_W5.1 Sparta, North Carolina, earthquake (abs.): Geological Society of America Abstracts with Programs, v. 56, no. 6, accessed September 28, 2021, https://gsa.confex.com/gsa/2020AM/meetingapp.cgi/Paper/361223.

Ma, X., and M. D. Zoback, 2020, Predicting lithology-controlled stress variations in the Woodford shale from well log data via viscoplastic relaxation: SPE Journal, v. 25, no. 5, p. 2534–2546, doi:10.2118/201232-PA.

Macqueen, R. W., and C. A. Sandberg, 1970, Stratigraphy, age, and interregional correlation of the Exshaw Formation, Alberta Rocky Mountains: Bulletin of Canadian Petroleum Geology, v. 18, no. 1, p. 32–66.

Madole, R. F., 1988, Stratigraphic evidence of Holocene faulting in the mid-continent: The Meers fault, southwestern Oklahoma: GSA Bulletin, v. 100, no. 3, p. 392–401, doi:10.1130/0016-7606(1988)100<0392:SEOHFI>2.3.CO;2.

Marra, K. R., S. B. Gaswirth, C. J. Schenk, H. M. Leathers-Miller, T. R. Klett, T. J. Mercier, P. A. Le, et al., 2017, Assessment of undiscovered oil and gas resources in the Spraberry Formation of the Midland Basin, Permian Basin Province, Texas, 2017: Washington, DC, US Geological Survey Fact Sheet 2017-3029, 2 p., 10.3133/fs20173029.

Marshak, S., K. E. Karlstrom, and J. M. Timmons, 2000, Inversion of Proterozoic extensional faults: An explanation for the pattern of Laramide and Ancestral Rockies intracratonic deformation, United States: Geology, v. 28, no. 8, p. 735, doi:10.1130/0091-7613(2000)28<735:IOPEFA>2.0.CO;2.

Marshak, S., W. J. Nelson, and J. H. McBride, 2003, Phanerozoic strike-slip faulting in the continental interior platform of the United States: Examples from the Laramide Orogen, midcontinent, and Ancestral Rocky Mountains: Geological Society, London, Special Publications 2003, v. 210, no. 1, p. 159–184, doi:10.1144/GSL.SP.2003.210.01.10.

Martini, A. M., L. M. Walter, J. M. Budai, T. C. W. Ku, C. J. Kaiser, and M. Schoell, 1998, Genetic and temporal relations between formation waters and biogenic methane: Upper Devonian Antrim Shale, Michigan Basin, USA: Geochimica et Cosmochimica Acta, v. 62, no. 10, p. 1699–1720, doi:10.1016/S0016-7037(98)00090-8.

Mazzotti, S., and J. Townend, 2010, State of stress in central and eastern North American seismic zones: Lithosphere, v. 2, no. 2, p. 76–83, doi:10.1130/L65.1.

Meissner, F. F., 1991, Petroleum geology of the Bakken Formation Williston Basin, North Dakota and Montana, *in* W. B. Hansen, ed., 1991 Guidebook to geology and horizontal drilling of the Bakken Formation: Billings, Montana, Montana Geological Society, p. 19–42, accessed August 30, 2020, http://archives.datapages.com/data/mgs/mt/data/0045/0019/0019.html.

Miller, B., J. Paneitz, M. Mullen, R. Meijs, M. Tunstall, and M. Garcia, 2008, The successful application of a compartmental completion technique used to isolate multiple hydraulic-fracture treatments in horizontal Bakken Shale wells in North Dakota: Society of Petroleum Engineers Annual Technical Conference and Exhibition, Denver, Colorado, September 21–24, 2008, p. 3992–4002, doi:10.2118/116469-MS.

Mitrovica, J. X., and W. R. Peltier, 1989, Pleistocene deglaciation and the global gravity field: Journal of Geophysical Research, v. 94, no. B10, p. 13651–13671, doi:10.1029/JB094iB10p13651.

Montgomery, S. L., 1997, Permian Bone Spring Formation: Sandstone play in the Delaware basin, part II—Basin: AAPG Bulletin, v. 81, no. 9, p. 1423–1434.

Montgomery, S. L., D. M. Jarvie, K. A. Bowker, and R. M. Pollastro, 2005, Mississippian Barnett Shale, Fort Worth basin, north-central Texas: Gas-shale play with multi-trillion cubic foot potential: AAPG Bulletin, v. 89, no. 2, p. 155–175, doi:10.1306/09170404042.

Mossop, G. D., and I. Shetsen, 1994, Introduction to the geological atlas of the Western Canada sedimentary basin, *in* G. D. Mossop and I. Shetsen, eds., Geological atlas of the Western Canada sedimentary basin: Calgary, Canada, Canadian Society of Petroleum Geologists and Alberta Research Council Calgary, p. 1–11.

Mount, V. S., and J. Suppe, 1992, Present-day stress orientations adjacent to active strike-slip faults: California and Sumatra: Journal of Geophysical Research, v. 97, no. B8, p. 11995, doi:10.1029/92JB00130.

Mullen, J., J. C. Lowry, and K. C. Nwabuoku, 2010, Lessons learned developing the Eagle Ford Shale: Tight Gas Completions Conference, San Antonio, Texas, November 2–3, 2010, SPE-138446-MS, p. 402–415, doi:10.2118/138446-MS.

National Energy Board, 2011, Tight oil developments in the Western Canada sedimentary basin: Energy briefing note: Calgary, Canada, National Energy Board, 36 p.

Nordquist, J. W., 1953, Mississippian stratigraphy of northern Montana, *in* J. M. Parker, ed., Billings Geological Society: Guidebook: Fourth Annual Field Conference: Billings, Montana, Montana Geological Society, p. 68–82.

Osadetz, K. G., A. Mort, L. R. Snowdon, D. C. Lawton, Z. Chen, and A. Saeedfar, 2018, Western Canada sedimentary basin petroleum systems: A working and evolving

paradigm: Interpretation, v. 6, no. 2, p. SE63–SE98, doi:10.1190/INT-2017-0165.1.

Patchen, D. G., and K. M. Carter, eds., 2015, A geologic play book for Utica Shale Appalachian basin exploration, final report of the Utica Shale Appalachian basin exploration consortium: Morgantown, West Virginia, West Virginia University, 187 p.

Peale, A. C., 1893, The Paleozoic section in the vicinity of Three Forks, Montana: Washington, DC, US Geological Survey Bulletin 110, 56 p., doi:10.3133/b110.

Peška, P., and M. D. Zoback, 1995, Compressive and tensile failure of inclined well bores and determination of in situ stress and rock strength: Journal of Geophysical Research: Solid Earth, v. 100, no. B7, p. 12791–12811, doi:10.1029/95JB00319.

Pindell, J. L., and L. Kennan, 2009, Tectonic evolution of the Gulf of Mexico, Caribbean and northern South America in the mantle reference frame: An update: Geological Society, London, Special Publications 2009, v. 328, no. 1, p. 1–55, doi:10.1144/SP328.1.

Pollastro, R. M., R. J. Hill, D. M. Jarvie, and M. E. Henry, 2003, Assessing undiscovered resources of the Barnett-Paleozoic total petroleum system, Bend Arch–Fort Worth Basin Province: AAPG Search and Discovery article 10034, accessed August 30, 2020, http://www.searchanddiscovery.com/pdfz/documents/pollastro/images/article.pdf.html.

Pollastro, R. M., D. M. Jarvie, R. J. Hill, and C. W. Adams, 2007, Geologic framework of the Mississippian Barnett Shale, Barnett-Paleozoic total petroleum system, Bend arch-Fort Worth Basin, Texas: AAPG Bulletin, v. 91, no. 4, p. 405–436, doi:10.1306/10300606008.

Quinones, L. A., H. R. DeShon, M. B. Magnani, and C. Frohlich, 2018, Stress orientations in the Fort Worth Basin, Texas, determined from earthquake focal mechanisms: Bulletin of the Seismological Society of America, v. 108, no. 3, p. 1124–1132, doi:10.1785/0120170337.

Rassouli, F. S., and M. D. Zoback, 2018, Comparison of short-term and long-term creep experiments in shales and carbonates from unconventional gas reservoirs: Rock Mechanics and Rock Engineering, v. 51, no. 7, p. 1995–2014, doi:10.1007/s00603-018-1444-y.

Reed, J. C., J. O. Wheeler, and B. E. Tucholke, 2005, Geologic map of North America: Decade of North American geology continental scale map 001: Boulder, Colorado, Geological Society of America, scale 1:5,000,000, 3 sheets, accessed August 30, 2020, https://www.usgs.gov/media/images/geologic-map-north-america.

Reiter, K., O. Heidbach, D. R. Schmitt, K. Haug, M. O. Ziegler, and I. Moeck, 2014, A revised crustal stress orientation database for Canada: Tectonophysics, v. 636, p. 111–124, doi:10.1016/j.tecto.2014.08.006.

Ricketts, J. W., K. E. Karlstrom, A. Priewisch, L. J. Crossey, V. J. Polyak, and Y. Asmerom, 2014, Quaternary extension in the Rio Grande rift at elevated strain rates recorded in travertine deposits, central New Mexico: Lithosphere, v. 6, no. 1, p. 3–16, doi:10.1130/L278.1.

Ricketts, J. W., S. A. Kelley, K. E. Karlstrom, B. Schmandt, M. S. Donahue, and J. van Wijk, 2016, Synchronous opening of the Rio Grande rift along its entire length at 25-10 Ma supported by apatite (U-Th)/He and fission-track thermochronology, and evaluation of possible driving mechanisms: Bulletin of the Geological Society of America, v. 128, no. 3–4, p. 397–424, doi:10.1130/B31223.1.

Ristau, J., G. C. Rogers, and J. F. Cassidy, 2003, Moment magnitude-local magnitude calibration for earthquakes off Canada's west coast: Bulletin of the Seismological Society of America, v. 93, no. 5, p. 2296–2300, doi:10.1785/0120030035.

Ristau, J., G. C. Rogers, and J. F. Cassidy, 2007, Stress in western Canada from regional moment tensor analysis: Canadian Journal of Earth Sciences, v. 44, no. 2, p. 127–148, doi:10.1139/e06-057.

Rittenhouse, S., J. Currie, and R. Blumstein, 2016, Using mud weights, DST, and DFIT data to generate a regional pore pressure model for the Delaware basin, New Mexico and Texas: Society of Petroleum Engineers/AAPG/Society of Exploration Geophysicists Unconventional Resources Technology Conference, San Antonio, Texas, August 1–3, 2016, p. 1243–1252.

Rocky Mountain Association of Geologists, 2014, Tectonic GIS data from the geological atlas of the Rocky Mountain Region: Denver, Colorado, Rocky Mountain Association of Geologists, 35 p.

Ross, D. J. K., and R. M. Bustin, 2008, Characterizing the shale gas resource potential of Devonian-Mississippian strata in the Western Canada sedimentary basin: Application of an integrated formation evaluation: AAPG Bulletin, v. 92, no. 1, p. 87–125, doi:10.1306/09040707048.

Rostami, E., N. Boness, and M. D. Zoback, 2020, Significance of well orientation on cumulative production from wells in the Bakken region: Proceedings of the 8th Unconventional Resources Technology Conference, Virtual, July 20–22, 2020, p. 734–747, doi:10.15530/urtec-2020-2813.

Ruppel, S. C., R. H. Jones, C. L. Breton, and J. A. Kane, 2005, Preparation of maps depicting geothermal gradient and Precambrian structure in the Permian basin: Washington, DC, US Geological Survey, https://www.beg.utexas.edu/files/publications/contract-reports/CR2005-Ruppel-2.pdf.

Ryder, R. T., C. S. Swezey, R. D. Crangle, and M. H. Trippi, 2008, Geologic cross section *E–E'* through the Appalachian basin from the Findlay arch, Wood County, Ohio, to the Valley and Ridge province, Pendleton County, West Virginia: Washington, DC, US Geological Survey Scientific Investigations Map 2985, 2 sheets, https://pubs.usgs.gov/sim/2985/.

Ryder, R. T., M. H. Trippi, C. S. Swezey, R. D. Crangle, R. S. Hope, E. L. Rowan, E. E. Lentz, 2012, Geologic cross section C–C' through the Appalachian basin from Erie County, north-central Ohio, to the Valley and Ridge province, Bedford County, south-central Pennsylvania: Washington, DC, US Geological Survey Scientific Investigations Map 3172, 2 sheets, https://pubs.usgs.gov/sim/3172/.

Sandberg, C. A., and C. R. Hammond, 1958, Devonian system in Williston basin and central Montana: AAPG Bulletin, v. 42, no. 10, p. 2293–2334, doi:10.1306/0BDA5BD0-16BD-11D7-8645000102C1865D.

Savvaidis, A., and P. H. Hennings, 2020, Preliminary report on the M4.9 earthquake in Culberson-Reeves County Line, version 3: Austin, Texas, Texas Data Repository, 16 p., doi:10.18738/T8/VHKAXV.

Savvaidis, A., B. Young, G. D. Huang, and A. Lomax, 2019, TexNet: A statewide seismological network in Texas: Seismological Research Letters, v. 90, no. 4, p. 1702–1715, doi:10.1785/0220180350.

Sbar, M. L., and L. R. Sykes, 1973, Contemporary compressive stress and seismicity in eastern North America: An example of intra-plate tectonics: Bulletin of the Geological Society of America, v. 84, no. 6, p. 1861–1882, doi:10.1130/0016-7606(1973)84<1861:CCSASI>2.0.CO;2.

Scales, M. M., H. R. DeShon, M. B. Magnani, J. I. Walter, L. Quinones, T. L. Pratt, and M. J. Hornbach, 2017, A decade of induced slip on the causative fault of the 2015 M_W 4.0 Venus Earthquake, Northeast Johnson County, Texas: Journal of Geophysical Research: Solid Earth, v. 122, no. 10, p. 7879–7894, doi:10.1002/2017JB014460.

Schmitt, G. T., 1954, Genesis and depositional history of Spraberry Formation, Midland basin, Texas: AAPG Bulletin, v. 38, no. 9, p. 1957–1978, doi:10.1306/5CEAE055-16BB-11D7-8645000102C1865D.

Schoenball, M., F. R. Walsh, M. Weingarten, and W. L. Ellsworth, 2018a, How faults wake up: The Guthrie-Langston, Oklahoma earthquakes: Leading Edge, v. 37, no. 2, p. 100–106, doi:10.1190/tle37020100.1.

Schoenball, M., F. R. Walsh, M. Weingarten, and W. L. Ellsworth, 2018b, Erratum to "How faults wake up: The Guthrie-Langston, Oklahoma earthquakes" [Leading Edge 37, no. 2 (2018) 100–106]: Leading Edge, v. 37, no. 3, p. 234, doi:10.1190/tle37030234b.1.

Schwab, D. R., T. S. Bidgoli, and M. H. Taylor, 2017, Characterizing the potential for injection-induced fault reactivation through subsurface structural mapping and stress field analysis, Wellington field, Sumner County, Kansas: Journal of Geophysical Research: Solid Earth, v. 122, no. 12, p. 10,132–10,154, doi:10.1002/2017JB014071.

Shen, L. W., D. R. Schmitt, and K. Haug, 2019, Quantitative constraints to the complete state of stress from the combined borehole and focal mechanism inversions: Fox Creek, Alberta: Tectonophysics, v. 764, p. 110–123, doi:10.1016/j.tecto.2019.04.023.

Simpson, R. W., 1997, Quantifying Anderson's fault types: Journal of Geophysical Research, v. 102, no. B8, p. 17909–17919, doi:10.1029/97JB01274.

Singh, A., S. Xu, M. D. Zoback, and M. McClure, 2019, Integrated analysis of the coupling between geomechanics and operational parameters to optimize hydraulic fracture propagation and proppant distribution: Society of Petroleum Engineers Hydraulic Fracturing Technology Conference and Exhibition, The Woodlands, Texas, February 5–7, 2019, SPE-194323-MS, 12 p.

Singh, S. K., J. F. Pacheco, X. Pérez-Campos, M. Ordaz, and E. Reinoso, 2015, The September 6, 1997 (M_W4.5) Coatzacoalcos-Minatitlán, Veracruz, Mexico earthquake: Implications for tectonics and seismic hazard of the region: Geofísica Internacional, v. 54, no. 3, p. 289–298, doi:10.1016/j.gi.2015.08.001.

Skinner, J. W., 1946, Correlation of Permian of west Texas and southeast New Mexico: AAPG Bulletin, v. 30, no. 11, p. 1857–1874, doi:10.1306/3D933887-16B1-11D7-8645000102C1865D.

Skoumal, R. J., R. Ries, M. R. Brudzinski, A. J. Barbour, and B. S. Currie, 2018, Earthquakes induced by hydraulic fracturing are pervasive in Oklahoma: Journal of Geophysical Research: Solid Earth, v. 123, no. 12, p. 10,918–10,935, doi:10.1029/2018JB016790.

Smith, J. P., 1929, The transitional Permian ammonoid fauna of Texas: American Journal of Science, v. s5-17, no. 97, p. 63–80, doi:10.2475/ajs.s5-17.97.63.

Smith, M. G., and R. M. Bustin, 2000, Late Devonian and Early Mississippian Bakken and Exshaw black shale source rocks, Western Canada sedimentary basin: A sequence stratigraphic interpretation: AAPG Bulletin, v. 84, no. 7, p. 940–960, doi:10.1306/A9673B76-1738-11D7-8645000102C1865D.

Sone, H., and M. D. Zoback, 2013, Mechanical properties of shale-gas reservoir rocks—Part 2: Ductile creep, brittle strength, and their relation to the elastic modulus: Geophysics, v. 78, no. 5, p. D393–D402, doi:10.1190/geo2013-0051.1.

Sone, H., and M. D. Zoback, 2014, Time-dependent deformation of shale gas reservoir rocks and its long-term effect on the in situ state of stress: International Journal of Rock Mechanics and Mining Sciences, v. 69, p. 120–132, doi:10.1016/j.ijrmms.2014.04.002.

Statler, A. T. 1965, Stratigraphy of the Simpson Group in Oklahoma: Tulsa Geological Society Digest, v. 33, no. 1955, p. 162–211, http://archives.datapages.com/data/tgs/digest/data/033/033001/162_tgs330162.htm.

Stoakes, F. A., 1980, Nature and control of shale basin fill and its effect on reef growth and termination: Upper Devonian Duvernay and Ireton formations of Alberta, Canada: Bulletin of Canadian Petroleum Geology, v. 28, no. 3, p. 345–410.

Sturm, S. D., and E. Gomez, 2009, Role of natural fracturing in production from the Bakken Formation, Williston basin, North Dakota: AAPG Search and Discovery article 50199, accessed August 30, 2020, http://www.searchanddiscovery.com/documents/2009/50199sturm/.

Swolfs, H. S., 1984, The triangular stress diagram—A graphical representation of crustal stress measurements: Washington, DC, US Geological Survey Professional Paper 1291, 19 p., doi:10.3133/pp1291.

Thomas, W. A., 2006, Tectonic inheritance at a continental margin: GSA Today, v. 16, no. 2, p. 4–11, doi:10.1130/1052-5173(2006)016[4:TIAACM]2.0.CO;2.

Thompson, R. C., 2015, Post-Laramide, collapse-related fracturing and associated production; Wind River basin, Wyoming: Rocky Mountain Geology, v. 52, no. 4, p. 27–46.

Tian, Y., W. B. Ayers, and W. D. McXain, 2013, Regional analysis of stratigraphy, reservoir characteristics, and fluid phases in the Eagle Ford Shale, south Texas: Gulf Coast

Association of Geological Societies Transactions, v. 62, no. 2010, p. 471–483, http://archives.datapages.com/data/gcags/data/062/062001/471_gcags620471.htm.

Townend, J., and M. D. Zoback, 2004, Regional tectonic stress near the San Andreas fault in central and southern California: Geophysical Research Letters, v. 31, no. 15, p. 1–5, doi:10.1029/2003GL018918.

US Energy Information Administration, 2014, Updates to the EIA Eagle Ford play maps: Washington, DC, US Energy Information Administration, 10 p., accessed August 30, 2020, https://www.eia.gov/maps/pdf/EIA%20Eagle%20Ford%20Play%20update%2012-29-14.pdf.

US Energy Information Administration, 2020, Drilling productivity report: For key tight oil and shale gas regions: Washington, DC, US Energy Information Administration, 11 p., accessed August 30, 2020, https://www.eia.gov/petroleum/drilling/archive/2020/01/.

US Geological Survey, 2020, M 5.1 – 4 km SE of Sparta, North Carolina, accessed March 8, 2021, https://earthquake.usgs.gov/earthquakes/eventpage/se60324281/executive.

US Geological Survey Earthquake Hazards Program, 2017, ANSS comprehensive earthquake catalogue (ComCat) documentation, accessed March 8, 2021, doi:10.5066/F7MS3QZH.

US Geological Survey Uinta-Piceance Assessment Team, 2003, Executive summary—Assessment of undiscovered oil and gas resources of the Uinta-Piceance Province of Utah and Colorado, 2002, *in* US Geological Survey Uinta-Piceance Assessment Team, ed., Petroleum systems and geologic assessment of oil and gas in the Uinta-Piceance Province, Utah and Colorado: Washington, DC, US Geological Survey Digital Data Series DDS-69-B, 3 p., doi:10.3133/ds69B.

Vavryčuk, V., 2014, Iterative joint inversion for stress and fault orientations from focal mechanisms: Geophysical Journal International, v. 199, no. 1, p. 69–77, doi:10.1093/gji/ggu224.

Vermylen, J., 2011, Geomechanical studies of the Barnett shale, Texas, USA, Ph.D. thesis, Stanford University, Stanford, California, 129 p.

Walsh, F. R., and M. D. Zoback, 2015, Oklahoma's recent earthquakes and saltwater disposal: Science Advances, v. 1, no. 5, p. e1500195, doi:10.1126/sciadv.1500195.

Walsh, W., C. Adams, B. Kerr, and J. Korol, 2006, Regional "shale gas" potential of the Triassic Doig and Montney Formations, northeastern British Columbia: Vancouver, Canada, British Columbia Ministry of Energy, Mines and Petroleum Resources Petroleum Geology Open File 2006-02, 19 p, http://cmscontent.nrs.gov.bc.ca/geoscience/publicationcatalogue/PetroleumGeosciencePublications/PGOF2006-02.pdf.

Warpinski, N. R., 1983, Investigation of the accuracy and reliability of in situ stress measurements using hydraulic fracturing in perforated cased holes: 24th US Symposium on Rock Mechanics, College Station, Texas, June 18–25, 1983, ARMA-83-0773, p. 773–786.

Warren, P. S., 1937, Age of the Exshaw Shale in the Canadian Rockies: American Journal of Science, v. s5-33, no. 198, p. 454–457, doi:10.2475/ajs.s5-33.198.454.

Wiggins, W. D., 1986, Geochemical signatures in carbonate matrix and their relation to deposition and diagenesis, Pennsylvanian Marble Falls limestone, central Texas: Journal of Sedimentary Petrology, v. 56, no. 6, p. 771–783, doi:10.1306/212F8A44-2B24-11D7-8648000102C1865D.

Wiltschko, D. V., and W. M. Chapple, 1977, Flow of weak rocks in Appalachian plateau folds: AAPG Bulletin, v. 61, no. 5, p. 653–670, doi:10.1306/C1EA3DBB-16C9-11D7-8645000102C1865D.

Wright, G. N., M. E. McMechan, D. E. G. Potter, G. D. Mossop, and I. Shetsen, 1994, Structure and architecture of the Western Canada sedimentary basin, *in* G. D. Mossop and I. Shetsen, eds., Geological atlas of the Western Canada Sedimentary Basin: Calgary, Canada, Canadian Society of Petroleum Geologists and Alberta Research Council Calgary, p. 25–40.

Xu, S., A. Singh, and M. D. Zoback, 2019, Variation of the least principal stress with depth and its effect on vertical hydraulic fracture propagation during multi-stage hydraulic fracturing: 53rd US Rock Mechanics/Geomechanics Symposium, New York, June 23–26, 2019, ARMA-2019-0254, 7 p.

Yang, W., and E. Hauksson, 2013, The tectonic crustal stress field and style of faulting along the Pacific North America plate boundary in southern California: Geophysical Journal International, v. 194, no. 1, p. 100–117, doi:10.1093/gji/ggt113.

Yang, W., E. Hauksson, and P. M. Shearer, 2012, Computing a large refined catalog of focal mechanisms for southern California (1981–2010): Temporal stability of the style of faulting: Bulletin of the Seismological Society of America, v. 102, no. 3, p. 1179–1194, doi:10.1785/0120110311.

Yang, Y., and M. D. Zoback, 2014, The role of preexisting fractures and faults during multistage hydraulic fracturing in the Bakken Formation: Interpretation, v. 2, no. 3, p. SG25–SG39, doi:10.1190/INT-2013-0158.1.

Zagorski, W. A., G. R. Wrightstone, and D. C. Bowman, 2012, The Appalachian basin Marcellus gas play: Its history of development, geologic controls on production, and future potential as a world-class reservoir, *in* J. A. Breyer, ed., Shale reservoirs—Giant resources for the 21st century: AAPG Memoir 97, p. 172–200, doi:10.1306/13321465M973491.

Zhang, H., D. W. Eaton, G. Rodriguez, and S. Q. Jia, 2019, Source-mechanism analysis and stress inversion for hydraulic-fracturing-induced event sequences near Fox Creek, Alberta: Bulletin of the Seismological Society of America, v. 109, no. 2, p. 636–651, doi:10.1785/0120180275.

Zhao, H., N. B. Givens, and B. Curtis, 2007, Thermal maturity of the Barnett Shale determined from well-log analysis: AAPG Bulletin, v. 91, no. 4, p. 535–549, doi:10.1306/10270606060.

Zoback, M. D., 2007, Reservoir geomechanics: Cambridge, United Kingdom, Cambridge University Press, 452 p.

Zoback, M. D., and A. H. Kohli, 2019, Unconventional reservoir geomechanics: Cambridge, United Kingdom, Cambridge University Press, 483 p.

Zoback, M. D., and J.-E. Lund Snee, 2018, Predicted and observed shear on preexisting faults during hydraulic fracture stimulation: Society of Exploration Geophysicists Technical Program Expanded Abstracts, Anaheim, California, October 16–19, 2018, p. 3588–3592, doi:10.1190/segam2018-2991018.1.

Zoback, M. D., J. Townend, and B. Grollimund, 2002, Steady-state failure equilibrium and deformation of intraplate lithosphere: International Geology Review, v. 44, no. 5, p. 383–401, doi:10.2747/0020-6814.44.5.383.

Zoback, M. D., M. L. Zoback, V. S. Mount, J. Suppe, J. P. Eaton, J. H. Healy, D. Oppenheimer, et al., 1987, New evidence on the state of stress of the San Andreas fault system: Science, v. 238, no. 4830, p. 1105–1111, doi:10.1126/science.238.4830.1105.

Zoback, M. L., 1992, First- and second-order patterns of stress in the lithosphere: The World Stress Map Project: Journal of Geophysical Research, v. 97 no. B8, p. 11703–11728, doi:10.1029/92JB00132.

Zoback, M. L., and M. D. Zoback, 1980, State of stress in the conterminous United States: Journal of Geophysical Research, v. 85, no. B11, p. 6113–6156, doi:JB085iB11p06113.

Zoback, M. L., and M. D. Zoback, 1989, Tectonic stress field of the continental United States, chapter 24, *in* L. C. Pakiser and W. D. Mooney, eds., Geophysical framework of the continental United States: Boulder, Colorado, Geological Society of America Memoir 172, p. 523–540, doi:10.1130/MEM172-p523.